2348 #4

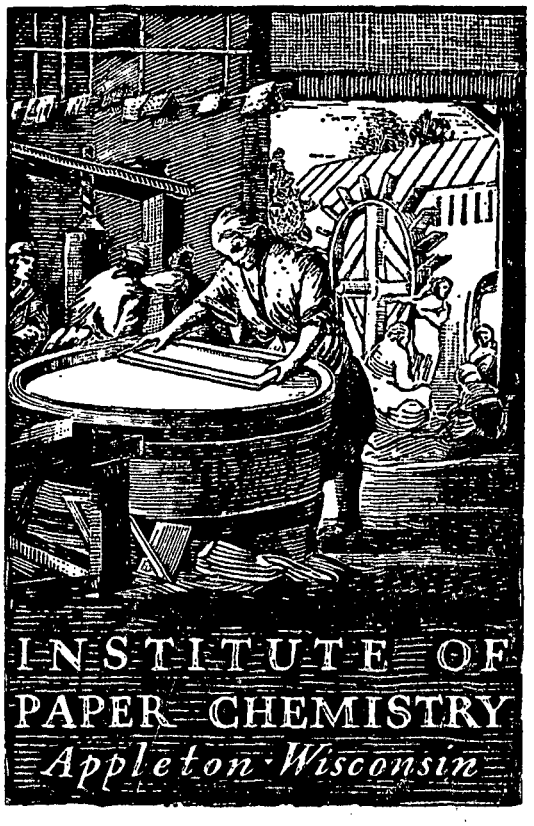

STUDIES OF THE SHEET-FORMING PROCESS

Forming Thin Mats of Wood Fibers at High Rates

Project 2348

Report Four

A Progress Report

to

MEMBERS OF GROUP PROJECT 2348

February 27, 1964

THE INSTITUTE OF PAPER CHEMISTRY
Appleton, Wisconsin

STUDIES OF THE SHEET-FORMING PROCESS

FORMING THIN MATS OF WOOD FIBERS AT HIGH RATES

Project 2348

Report Four

A Progress Report to

MEMBERS OF GROUP PROJECT 2348

February 27, 1964

Members of Group Project 2348:

Consolidated Papers, Inc.

Crown Zellerbach Corporation

Eastman Kodak Company

The Eaton-Dikeman Company

P. H. Glatfelter Co.

International Paper Company

Kimberly-Clark Corporation

KVP Sutherland Paper Company

Longview Fibre Company

Marathon Division, American Can Company

The Mead Corporation

Personal Products Company

Riegel Paper Company

St. Regis Paper Company

Scott Paper Company

Union Bag-Camp Paper Corporation

West Virginia Pulp & Paper Company

TABLE OF CONTENTS

THE INSTITUTE OF PAPER CHEMISTRY
Appleton, Wisconsin

STUDIES OF THE SHEET-FORMING PROCESS

FORMING THIN MATS OF WOOD FIBERS AT HIGH RATES

SUMMARY

The previous work in relating flow conditions, fluid properties, and fiber properties in the permeation and formation of thin mats of synthetic fibers has been extended to fines-free wood pulp fibers. The additional complications encountered in wood pulps are concerned with the heterogeneous nature of irregularly shaped and water-swollen fibers and fiber mats of much greater compressibility. This greater compressibility has been found to be responsible for much more severe fiber-wire interaction phenomena than was encountered previously with less compressible synthetic fibers.

The problem of fiber characterization was studied in two ways: (1) microscopically and by determining the average fiber mass, and (2) hydrodynamically by evaluating the fiber specific surface and swollen specific volume from the average porosity flow correlation applied to the viscous flow regime. The results of these studies with a classified bleached sulfite pulp indicated that although there was a systematic deviation of the experimental data from the viscous flow correlation, the values of specific surface and specific volume calculated from the hydrodynamic data agreed remarkably well with those determined microscopically and from the average fiber mass.

In the analysis of possible reasons for the discrepancies between the data and the viscous flow correlation, it was reasoned that the probable errors in neglect of the contact area of wood pulp fibers in compacted mats and neglect of possible influence of fiber shape on flow resistance approximately counterbalance

one another in the use of a Kozeny factor-porosity relationship empirically determined for uniform cylindrical fibers. Thus, it was speculated that the remaining possible reason for deviations of the data from the flow correlation is due to a dependency of swollen fiber specific volume on fluid stress. The value of specific volume which is evaluated from hydrodynamic data probably represents an average over the pressure drop range in which the data are correlated. However, over a range of practical interest from about 10 to 100 cm. of water frictional pressure drop, the viscous flow correlation represents the experimental results with an error less than $\pm 10\%$. Since this uncertainty is within the precision of about $\pm 15\%$ of the flow correlation itself, the use of hydrodynamic evaluation of specific surface and specific volume and the use of mechanical compacting pressure measurements to characterize fiber mat compressibilities are justified from both an empirical accuracy standpoint and from the fact that the fiber properties appear to have real physical significance.

Although the average porosity concept used in the previous development of an integrated flow correlation representing both viscous and inertial resistance of fiber mats under fluid stress cannot be rigorously derived, average porosity is precisely defined to agree with experimentally measured mat permeabilities. The results of numerical integration of the differential form of the flow equations showed the use of the average porosity concept to be valid. Since fiber properties themselves are determined from the use of the average porosity concept and precise determination of over-all flow data, the minor and constant errors occasioned by use of the average porosity integrating factor for thick mats are minimized and analysis of flow data with the differential form of the correlation is not justified from accuracy or precision arguments.

However, one serious limitation in the use of the average porosity correlation for wood pulp fibers was found because of greater compressibility of wood pulp fiber mats as compared to synthetic fibers. At pressure drops greater than about 200 cm. of water, wood pulp fiber mat porosities near the forming wire are about 0.6 . At higher pressure drops, the average porosity correlation indicates a spurious maximum in flow velocity and then a decrease as frictional pressure drop is further increased. Physically, this situation cannot exist, but results from the numerical breakdown of the integrating factor in the flow correlation as very low porosities are approached.

On the other hand, numerical integrations of the differential form of the flow correlation indicate a more realistic approach of an infinite pressure drop as flow velocities are increased to a point where the mat porosity at the forming wire is approaching zero (at about 1500 cm. of water for wood pulp fibers). Comparison of permeation data for mats of fixed basis weights at high velocities and high pressure drops greater than about 200 cm. of water with the numerically integrated flow correlation show that a significant fiber deswelling probably occurs at these high pressure drops. The result is that the porosities of actual mats near the forming wire are larger than those predicted from the static compressibility data assuming that the swollen fiber specific volume remains constant. Therefore at high pressure drops, the numerically integrated flow correlation predicts too rapid an increase in pressure drop with increasing flow velocity as porosities of zero are approached.

Considerable difficulty in interpretation of permeation experiments on wood fiber mats is caused by decay of permeability phenomena, which is manifested by either a time-dependent increase in frictional pressure drop at constant flow rate or a time-dependent decrease in flow rate at constant over-all frictional

pressure drop. In one set of experiments where it was possible to eliminate water impurities as a source of decay of permeability, it was demonstrated that mechanical conditioning of the mat under small cyclical flow variations was probably the main reason for observed decay phenomena. It was demonstrated that a mat could be mechanically conditioned by cyclical application of fluid stress until an equilibrium condition was reached in which no further decay could be observed. Fiber mats were also mechanically conditioned by application of cyclical mechanical compacting pressures in which the same number of cycles were required as in the previous fluid mechanical conditioning experiments. Although the results of the compression data for mechanically conditioned mats could possibly explain the higher resistance of the mechanically conditioned mats compared to mats not previously subjected to high fluid stresses, it was still possible for a time-dependent fiber deswelling to contribute significantly to decay phenomena.

Because of the difficulty in eliminating decay of permeability from both mechanically conditioning effects and trace impurities in the water supply system, further attempts at obtaining permeation data for highly compressible wood pulp fiber mats were abandoned. Further hydrodynamic data were obtained in the dynamic drainage tester where short filtration times (less than 4 seconds) minimize any decay effects.

Hydrodynamic data characterizing the continuous formation of thin mats from essentially zero to about 70 g./m.^{2} were obtained with the previously developed dynamic drainage tester for velocities up to about 100 cm. per sec. with classified bleached sulfite pulp. In agreement with previous studies, it was observed that the data showed higher pressure drops at a given basis weight than would be predicted from the average porosity flow correlation. In the case of these studies with wood pulp fibers, the discrepancies at low basis weights were

much more serious than previously found in the investigations of less compressible synthetic fibers. Although it appeared probable that the previously found three major reasons for the discrepancies were caused by (1) a changing porosity distribution in thin mats, (2) flow convergence because of the presence of forming wire, and (3) probable change of mat compressibility with decreasing basis weight, the more compressible wood pulp fibers definitely made the changing porosity distribution effect much more important for wood pulp fibers than for less compressible synthetic fibers.

On the assumption that a changing porosity distribution in thin fiber mats was the controlling effect, an empirically defined porosity distribution factor was calculated from the data and could then be used to satisfactorily correlate the data over the entire velocity and basis weight range and up to frictional pressure drops of about 150 cm. of water. The results of the analysis and the experiments indicated that for wood pulp fiber mats of basis weights greater than about 100 g. per $m.^2$ the porosity distribution could be satisfactorily predicted by the previously established flow correlation. At lower basis weights, a significant fiber-wire interaction occurs and it is necessary to obtain data to empirically characterize the porosity distribution factor.

The quantitative relationships used in the analysis of the data and developed from interpretation of the experiments are summarized below.

Modified Hydraulic Radius Flow Correlation. The following quantitative relationship is applicable to flow of a fluid through porous media in general and relates fluid and porous media properties to flow conditions:

$$\frac{\Delta P}{W/A} = \left[\frac{\bar{k}(1-\bar{\epsilon})}{\bar{\epsilon}^3}\right] v S_v^2 \mu U + b' \left[\frac{\sqrt{\bar{k}}}{\bar{\epsilon}^3}\right] v S_v \rho U^2 \qquad (8).$$

Flow conditions:

ΔP = frictional pressure drop,

U = superficial fluid velocity,

b' = coefficient of inertial resistance.

Fluid properties:

μ = fluid viscosity,

ρ = fluid density.

Porous medium properties:

W/A = mass per unit area (basis weight),

v = particle specific volume,

S_v = particle specific surfate,

$\bar{\epsilon}$ = average porosity,

$\bar{k}$ = Kozeny factor based on average porosity.

Auxiliary Equations for Fibrous Systems. The following relationships are used with Equation (8) when applied to fiber mats:

Kozeny factor:

$$\bar{k} = \frac{3.5\bar{\epsilon}^3}{(1 - \bar{\epsilon})^{1/2}}[1 + 57(1 - \bar{\epsilon})^3] \qquad (7),$$

Average porosity:

$$\bar{\epsilon} = 1 - Ivc_p \qquad (13),$$

Porosity distribution factor:

$$I = (1 - \frac{N}{2})^2 + (N - \frac{N^2}{4})e^{-252(W/A)} \qquad (14),$$

Fiber mat compressibility:

$$c_p = M\Delta P^N \qquad (4),$$

Coefficient of inertial resistance:

$$b' = 0.1 .$$

Approximate Empirical Correlation. By force-fitting the hydrodynamic data, an approximate equation may be used to facilitate quick numerical estimates of wood pulp behavior over the stipulated range of variables:

$$\Delta P = k' U^n (W/A)^m .$$

Numerical values:	Range:
$k' = 1.68 \times 10^4$	$10^4 < \Delta P < 10^5$ dynes/cm.^{2}
$n = 2.60$	$10 < U < 100$ cm./sec.
$m = 1.46$	$10^{-3} < (W/A) < 10^{-2}$ g./cm.^{2}

INTRODUCTION

Reports One (1) and Two (2) of Project 2348 on "Studies of the Sheet-Forming Process" were concerned with initial investigations of the filtration and permeation of thin mats formed from synthetic fibers. In Report Two (2) it was demonstrated that previously presented flow correlations based on a modified hydraulic radius theory for thick fiber mats held within about 15% down to basis weights as low as 50 g./m.^{2} Below 50 g./m.^{2} basis weight, there was evidence of the effect of fiber-wire interaction. In the analysis of the data, it was concluded that two controlling effects tended to give experimental values of pressure drop larger than those predicted from the flow correlation after correcting for the resistance of the bare forming wire: (1) changing porosity distributions in thin fiber mats because of an approach to uniform porosity and changing mat compression with decreasing basis weight, and (2) flow convergence phenomena in the thin fiber mats because of the presence of the forming wire affecting fluid motion in the mat.

In Report One (1), a dynamic drainage tester was instrumentated and tested for forming thin fiber mats at constant drainage rates and short forming times. Mat formation was characterized by the recording of an oscilloscope trace of frictional pressure drop over the mat and wire as a function of forming time. It was demonstrated that acceleration effects were negligible at forming times of less than 0.05 second and that measurements of mean speed and pressure were reliable. The initial sheet-forming tests conducted with dacron fibers in dilute suspensions agreed with the previously developed flow correlation for thick mats within 10%.

Because of the success in correlating the data for the formation of thin synthetic fiber mats, it was decided to proceed with permeation and filtration tests on a carefully selected wood pulp. It was anticipated that new phenomena

might be encountered because of the greater flexibility of wood pulps as compared to synthetic fibers, and because of the more complicated shape and internal structure of wood pulps. Because of serious complications encountered in decay in permeability of wood pulp fiber mats under the sustained flow conditions necessary in the permeation tester, only a limited amount of permeation data were obtained for this report. Most of the data presented here are concerned with the problem of wood pulp fiber characterization and analysis of sheet-forming data in the dynamic drainage tester where, under short filtration time conditions, decay effects are not important.

EXPERIMENTAL

The experimental work can be divided into three main classifications of (1) fiber characterization, (2) permeation tests, and (3) dynamic drainage or filtration tests. The fiber chosen for study was bleached sulfite pulp consisting mainly of spruce and hemlock fibers.

FIBER PREPARATION

A commercially prepared dry-lap form of the pulp was torn into about 1-inch squares and soaked in water for 48 hours at room temperature. The stock at a consistency of about 1.6% was then slushed for 5 minutes in a 5.5-lb. laboratory Valley beater with no bedplate load. Following this disintegration, the stock was dewatered by vacuum filtration to about 20% o.d. and then classified in a Bauer-McNett classifier. The only modifications in the Bauer-McNett apparatus were to nickel-plate the flow chambers of the apparatus to minimize the possibility of pulp contamination from corrosion products and to replace the rubber drive belts with nylon belts to prevent contamination from rubber particles. The four sets of screens used were 14, 28, 35, and 65-mesh. A 15-gram charge of pulp was classified for 30 minutes in the Bauer-McNett equipment, and all fines and fibers passing through the 35-mesh screen were discarded. The fibers retained in the other classifier chambers were combined and dewatered by vacuum filtration.

The dewatered fiber mat was reduced in size in a pulp shredder and stored in polyethylene bags at about 34°F. About 1% formaldehyde was added to each bag to minimize possible bacterial action during storage. Several pounds of the bleached sulfite fibers were prepared in the above manner and stored at a moisture content of 29.17% o.d.

FIBER CHARACTERIZATION

The fiber properties that affect resistance to drainage are the external surface area, the swollen fiber specific volume, and the fiber mat compressibility. Fibers were prepared for testing in all cases by first putting them into aqueous dispersion in the following manner. A slurry prepared at about 0.5% consistency was uniformly dispersed in a British disintegrator for a minimum period of 7500 revolutions (300 counts), and then was deaerated under water pump suction for 30 minutes.

Fiber mat compressibility was determined in a static compression tester on thick mats with basis weights of about 2000 g./m.^{2} The slurry at about 0.5% consistency was placed in a 3-inch i.d. Lucite tube and thoroughly dispersed to prevent gross flocculation. A permeable piston of known weight and volume was then carefully lowered on the suspension in such a manner that the internal pressure in the slurry never exceeded 1-2 centimeters of water. A micrometer arrangement on the piston shaft was used to measure compressed mat thickness as a function of applied load. Readings of mat thickness were taken when the rate of change of mat thickness with time at a given mat load was less than 0.001 cm. per minute. Loads from 10 to about 150 g./cm.^{2} were used in the compression tests. To transform the thickness-load data to mat apparent density versus compacting pressure, an accurate measure of mat weight was obtained following the compression measurements by drying the wet pad for 24 hours at 105°C.

In previous studies of synthetic fibers, the fiber specific surface and specific volume could be determined directly and accurately by microscopic and pycnometer measurements. In the case of water-swollen and irregularly shaped wood fibers, direct microscopic observations are more complex and less accurate. However, to obtain checks on the physical significance of specific surface and

specific volume calculations made from more precise hydrodynamic measurements, a series of microscopic determinations were made in the following manner.

It was desired to prepare fiber cross sections in as nearly a water-swollen condition as possible. The disintegrated pulp sample was first stained with a 2% solution of Congo Red dye to facilitate viewing. The stained sample was then filtered, washed, and diluted with distilled water so that 1 drop of suspension from a 6-mm. i.d. pipet contained approximately 50 fibers. The fibers were then bundled together in parallel orientation under a Greenough-type binocular microscope with the aid of dissecting needles.

To allow subsequent handling of the fiber bundles it was necessary to allow them to partially dry on a glass slide. The partially bonded fiber bundles were then placed in a glass vial containing absolute alcohol for 30-40 minutes. They were then transferred to Epon 812 resin for 30-40 minutes, and finally placed in a mixture of equal parts of Epon 812 and Epoxy Hardener DDSA (dodecenyl succinic anhydride) for 30-40 minutes.

The fiber bundles were then transferred to gelatin capsules filled with a solution consisting of 10 ml. of Epon 812, 90 ml. of DDSA Hardener, and 1% BDMA Accelerator (benzyldimethylamine). The capsules were placed in a 50°C. oven for approximately 24 hours until the resin had polymerized.

Cross sections, 10 microns in thickness, were prepared on a sliding microtome at approximately the middle of the fiber bundles. The Epoxy sections were flattened on a glass slide with toluene and then mounted in Canada balsam. Tracings of fiber images projected on the ground glass of a photographic camera were made at a magnification of 750 diameters. Tracings of three separate fiber bundles were made.

Although it was hoped that fiber cross sections prepared in the above manner would be in a nearly water-swollen condition, it was recognized that some unknown amount of shrinkage had occurred in the partial drying of the fiber bundles. In addition, there was probably some slight fiber shrinkage because of the volume shrinkage of the epoxy resin of approximately 1-2% during polymerization.

Fiber length determinations were made on the air-dried fibers by projecting the fiber images at a magnification of 50X and then determining the individual fiber lengths with the Finnish Fiber Length Recorder. Since the shrinkage of fibers in the axial direction during drying is known to be relatively small, it was felt that the lengths of dry fibers would be very closely representative of the lengths of water-swollen fibers.

In addition to fiber cross section and length distributions, it was necessary to determine the average fiber mass in the translation of the microscopic results to surface and volume values on a mass basis (specific surface and specific volume). Some previous experiments with Graff's (3) dilution technique for determining average fiber mass had indicated the possibility of errors occasioned by fiber processing and fiber classification during dilution. Therefore, the following modified technique was developed.

The wet pulp sample was solvent exchanged using ethyl alcohol of increasingly higher percentages until the final exchange was made with absolute alcohol. Fibers were then dried at 105°C. and stored in a desiccator. Two samples of approximately 0.6 gram each were weighed and dispersed in distilled water under vacuum for 24 hours. A sample was then transferred to a large stainless steel dilution tank and further diluted to 16 liters. Complete dispersion at this consistency was accomplished by gentle stirring at slow speed with a small Lightnin' mixer for five minutes. Then two samples of 600 milliliters each were withdrawn

and again diluted to 16 liters. Following 5-minute mixing, two final samples of 100 milliliters each were removed from the mixing vessel and placed in separate 150-milliliter Petri dishes. A hot agar solution was added to solidify the mixture and the number of fibers in each sample was counted under the microscope. Fiber classification during the removal of aliquot samples was carefully minimized by using wide-mouthed beakers as the sampling vessels. The exact amounts of slurry removed during the sampling steps were determined by direct weighing.

Carefully controlled constant-rate filtrations were made in the viscous flow regime (4) to obtain an accurate pressure drop-versus-time record of the fiber mat buildup for the purpose of calculating the water-swollen fiber specific surface and specific volume. A schematic diagram of the flow equipment is shown in Fig. 1. The deaerated and dispersed fiber sample prepared as previously described was diluted to about 0.01% consistency and carefully mixed in a 100-liter slurry feed tank for about five minutes. The slurry was admitted to the filtration tube and maintained at a constant liquid level with a float device which electronically controlled a Saunders-type valve on the slurry feed line.

The filtration was commenced by actuating the preset eddy clutch drive controlling the gear pump speed on the downstream side of the septum. Flow rate was measured with a calibrated rotameter, and minor flow adjustments with the potentiometer were made during the run to maintain a constant rate of flow as the pressure drop increased over the mat formed in the filtration tube. Downstream pressures were measured with a bellows-type gage connected to a Microsen balance and recorded directly on a strip chart potentiometric-type recorder of 0.5-second full-scale response. Slurry temperature was measured in the filtration tube to the nearest 0.1°C. during the run. When the final pressure drop reached 95 centimeters of water, the tube was drained and the mat weight determined by

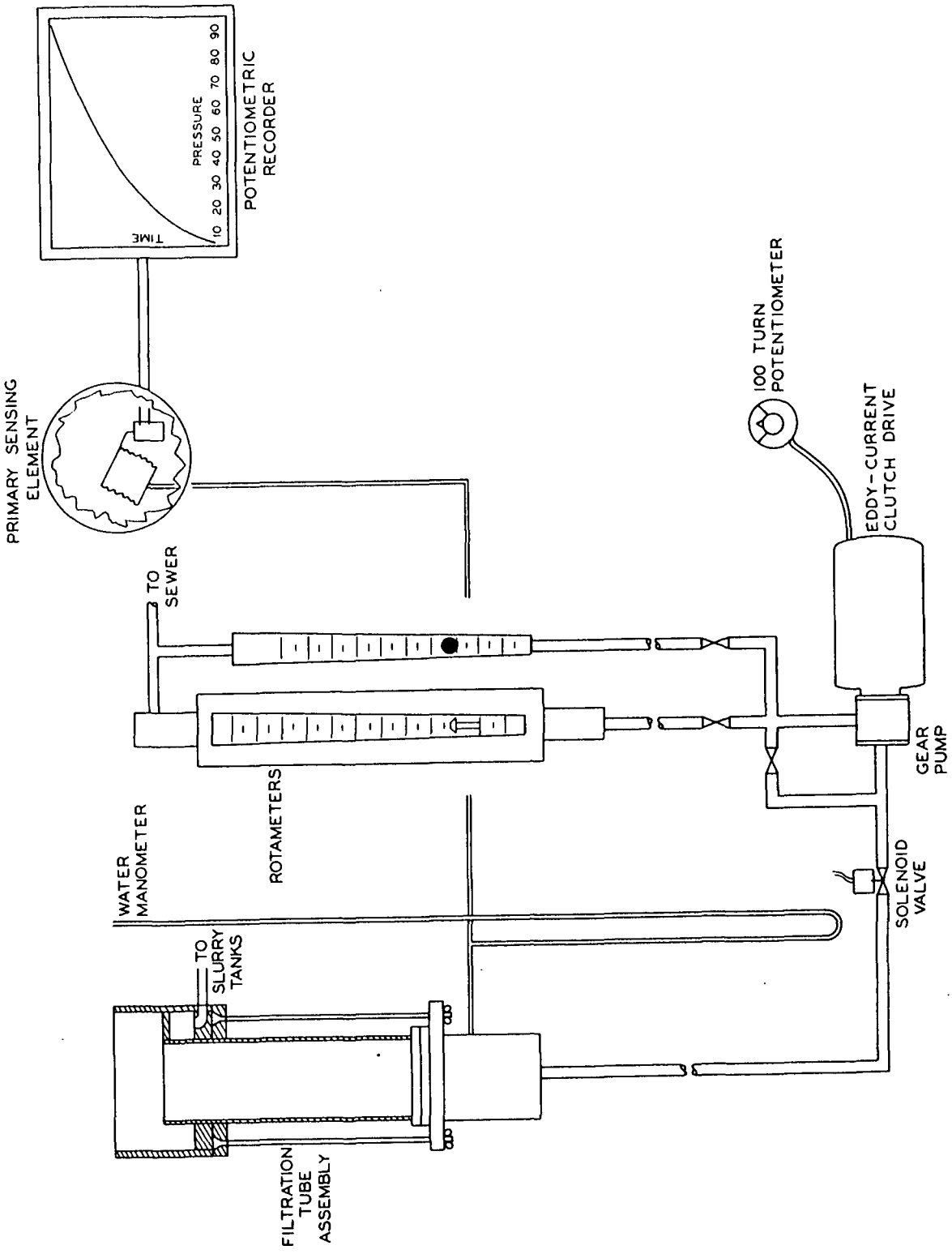

Figure 1. Viscous Flow Constant-Rate Filtration Apparatus

weighing after drying at 105°C. Slurry consistency was determined from the final mat weight and total metered slurry volume. The bypass flow system indicated in Fig. 1 around the gear pump was used to control the back pressure at about 20 lb./in.^{2} to minimize changes in flow rate as the pressure drop across the mat increased during the run.

PERMEATION TESTS

The permeation tester and procedures for studying flow resistance of bare forming wires and preformed fiber mats of fixed basis weights has been described previously (2, 4) in detail. The same general procedures have been used in this study of a classified wood pulp fiber.

Briefly, the forming wire selected was a 100-mesh, plain-weave wire (Tyler) screen whose wire diameter was 0.0045 in. and screen thickness 0.0098 in. This forming wire was backed by a 35-mesh, plain-weave wire on a perforated and countersunk brass disk of about 80% open area. The holes in the brass disk were 1/4-inch diameter on 5/16-inch centers. The frictional pressure drop-velocity relationship for this forming wire-backing plate combination was determined and is given in Appendix V.

Fiber mats were formed at various basis weights on the wire screen and then permeated with water until an apparent equilibrium frictional pressure drop was reached. Readings of flow velocity and pressure were taken as quickly as possible to minimize decay-of-permeation effects over a velocity range up to 160 cm./sec.

Elaborate precautions were taken in the cleaning of the entire water supply and flow system and in the preparation of water for use in mat permeation to minimize decay of permeability because of entrapment of trace impurities within the

fiber mat over periods of sustained flow in the permeation tester. Freshly prepared distilled water was used for each series of permeation runs at a pH of 6.5 and a conductivity of about 1 micromho.

In the early permeation testing work, small amounts of formaldehyde were added to the contents in the supply tank to minimize possible bacterial action since it was known that very small amounts of volatile organic residues were still present in the distilled water. Several permeability runs were made in which no obvious decay in permeability occurred from impurities in the water. However, after the initial testing it was observed that significant quantities of impurities were leading to slight discoloration of the fiber mats following completion of runs. After a thorough investigation of the possible sources of the impurities, the trouble was traced to a fungous and bacterial growth in the flow system. The most effective agent of the various fungicides and bactericides employed to combat this growth was found to be phenyl mercuric acetate (PMA). It was necessary to use massive doses of PMA to stop further fungous growth, but, at this point, previously deposited impurities of fungous origin began to be removed slowly from the walls of the piping system and storage vessels. Exhaustive and drastic cleaning procedures and techniques were tried unsuccessfully in attempts to remove residual fungus and bacteria. However, subsequent permeation tests always showed evidence of decay in permeability as indicated by slight mat discoloration from these materials. Only those initial permeation tests in which no decay of permeability caused by impurities in the water were used for analysis in this report.

DYNAMIC DRAINAGE TESTER

The calibration, instrumentation, and operation of the dynamic drainage tester in the forming of thin synthetic fiber mats has been reported previously in detail (1). In brief summary, the tester consists of a 3-inch diameter flow tube

in which a piston is moved at constant speed to form a mat in the upstream portion of the tube. The pressure drop across the combination of mat and forming wire with backing plate is measured by a strain gage in the upstream portion of the tube wall.

The testing procedures described in Report One (1) were followed in this study with one exception: Instead of recording the amplified pressure signal by photographing an oscilloscope trace, the amplified signal from the strain gage was recorded on an Offner Type RS one-channel Dynograph. The deflection time specification of this high-speed recorder is 2.5 milliseconds. An example of the type of pressure trace obtained with this instrument is given in Appendix V together with a sample calculation for one of the runs made in the dynamic drainage tester.

The same type of forming wire, backing wire, and brass septum were used in the dynamic drainage tester as in the permeability tester. The screen calibration previously obtained in the permeability tester was checked in the dynamic drainage tester. Because of the greater accuracy of the pressure drop data from the permeability tester, the bare wire resistance curve given in Appendix V from the permeability tester was used to correct the measured over-all pressure trace from the recorder to give the pressure drop over the fiber mat as a function of forming time. Flow velocities were determined from the known distance of piston travel and measured time of travel. Slurry consistencies were calculated from the known tube volume and the weighed fiber mass following completion of the test. Slurry temperatures in the supply tank were maintained at about room temperature and measured in the supply tank.

To cover a velocity range of about 20-100 cm./sec. in the dynamic drainage tester experiments, two slurry consistencies of ca. 0.01 and 0.004% were used, covering basis weight ranges of 0-70 and 0-30 g./m.^{2}, respectively. Forming times could be read with negligible acceleration effects, as previously determined, down to as low as about 0.02 sec. (1).

RESULTS AND DISCUSSION

The first part of this section presents the fiber characterization data from microscopic measurements and fiber mass determination. Next, the evaluation of the fiber properties of specific surface and specific volume from mat compression data and hydrodynamic data in the viscous flow regime are discussed. The next part of the data deals with high-velocity water-flow permeation studies with particular reference to decay of permeability phenomena. Finally, the results of dynamic drainage tests in which thin fiber mats are formed at constant rates are analyzed.

FIBER DIMENSIONS AND MASS

The objectives in this part of the work are to obtain independent measurements of the important wood pulp fiber properties that are needed to calculate the fiber hydrodynamic properties affecting drainage. The specific surface of the fibers may be calculated from measurements of fiber perimeter, fiber length, and fiber mass by dividing the external area per fiber by the mass per fiber. The specific volume is evaluated by multiplying the cross-sectional area per fiber by the length per fiber and dividing this fiber volume by the mass per fiber.

Figure 2 shows the classified bleached sulfite fiber cross sections. The fibers have an irregular, flattened shape of roughly elliptical form. The relatively high extent of lumen collapse in a number of the fibers indicates that the partial drying step in the preparation of the water-swollen cross sections may have been responsible for a reduction in fiber volume over that representative of a completely water-filled lumen.

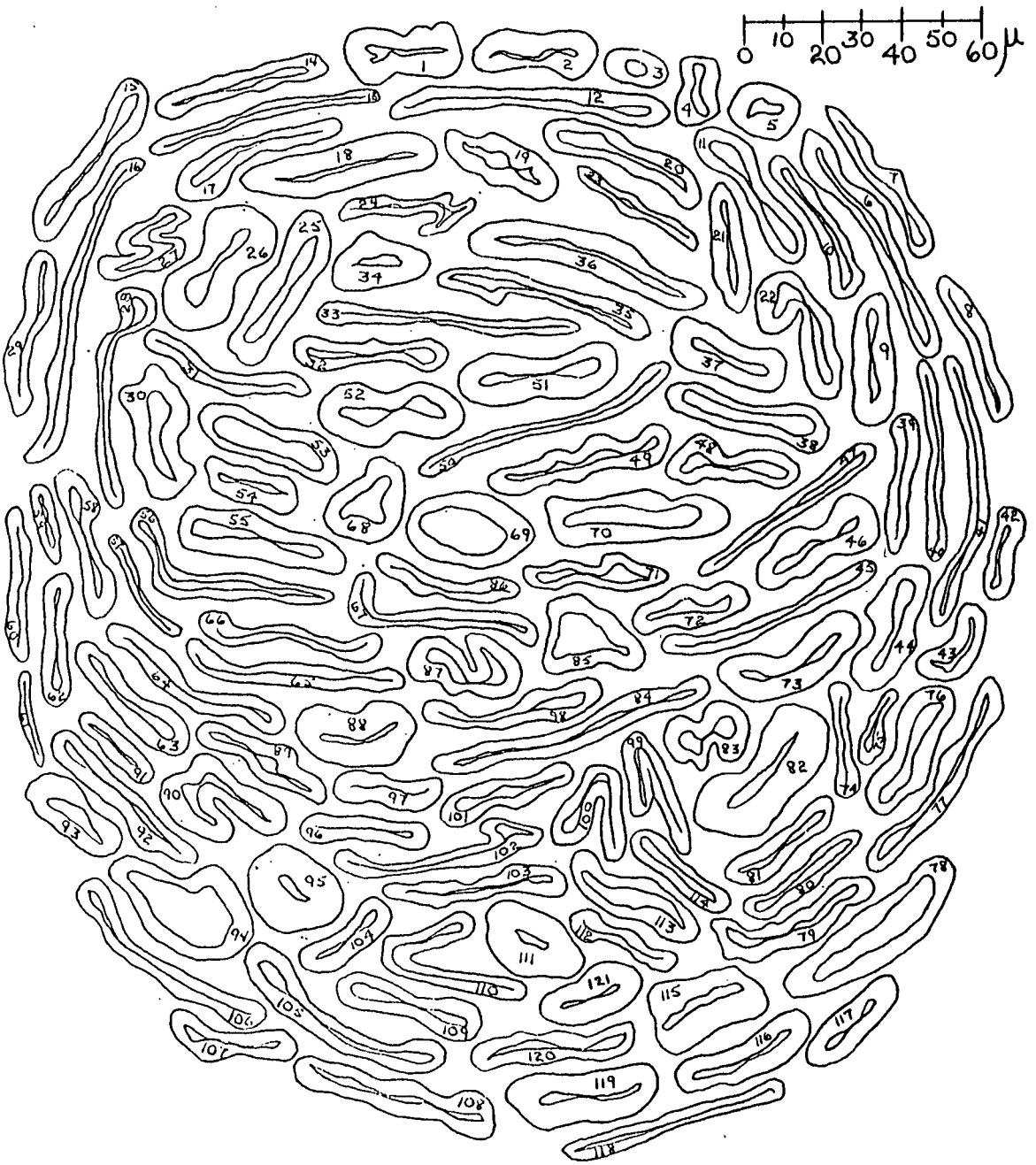

Figure 2. Classified Bleached Sulfite Fiber Cross Sections (600X)

The fiber perimeter measurements based on the cross sections of 121 fibers in Fig. 2 are given in Appendix I, Table I-I, and the approximate perimeter frequency distribution curve is shown in Fig. 3. The smallest measured perimeter was 46 microns, whereas the largest was 180 microns. The distribution curve shows that the arithmetic average perimeter of 95 microns is larger than the peak value of 83 microns.

The arithmetic average fiber cross-sectional area was determined by cutting out each fiber cross section from tracing paper, weighing them, and dividing the total weight by the basis weight of the paper and the number of fibers (121) and finally correcting for the magnification factor. The arithmetic average cross section so obtained was 2.90×10^{-6} cm.^{2} per fiber.

The fiber length distribution curve is shown in Fig. 4 and is based on the data in Appendix I, Table I-II. As in the case of perimeter distribution, the frequency distribution of length is also skewed, with the arithmetic average being 2.04 mm. compared to the peak value of 1.52 mm. Fibers as short as 0.1 mm. and as long as 5 mm. were measured.

The arithmetic average fiber mass as determined from the modified dilution technique was 3.61×10^{-7} g., which corresponds to 2.78 million fibers per gram. The results of four separate counts of about 400 fibers were in good agreement, as indicated in Appendix I, Table I-III. The precision of the modified technique is good with an average deviation from the mean of about 2%.

The above fiber dimensions and fiber mass are summarized in Table I together with calculated values of specific surface and specific volume. In addition, fiber widths, defined as the longest cross-sectional dimension, were measured and used to calculate the equivalent fiber thickness from the measured

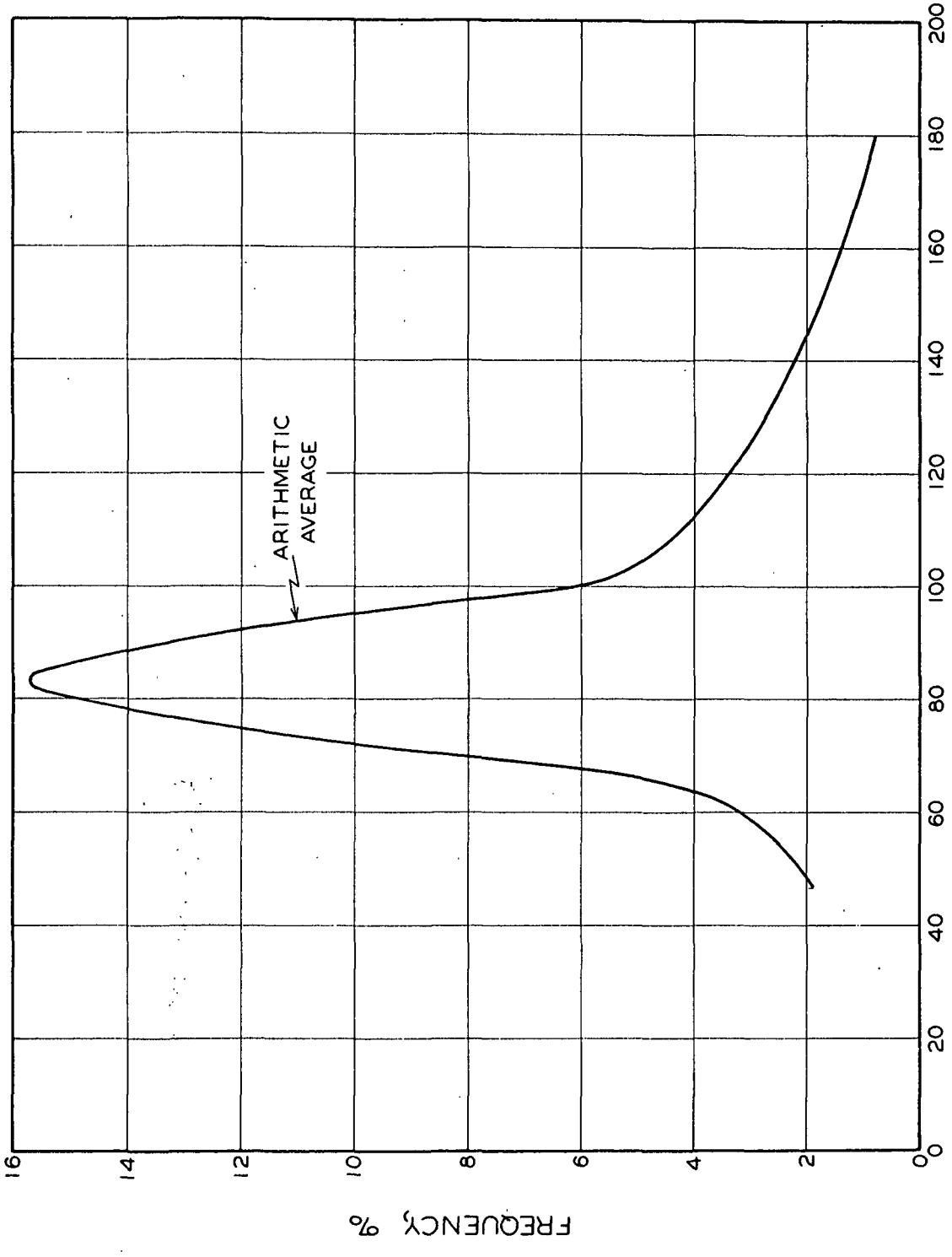

Figure 3. Fiber Perimeter Distribution

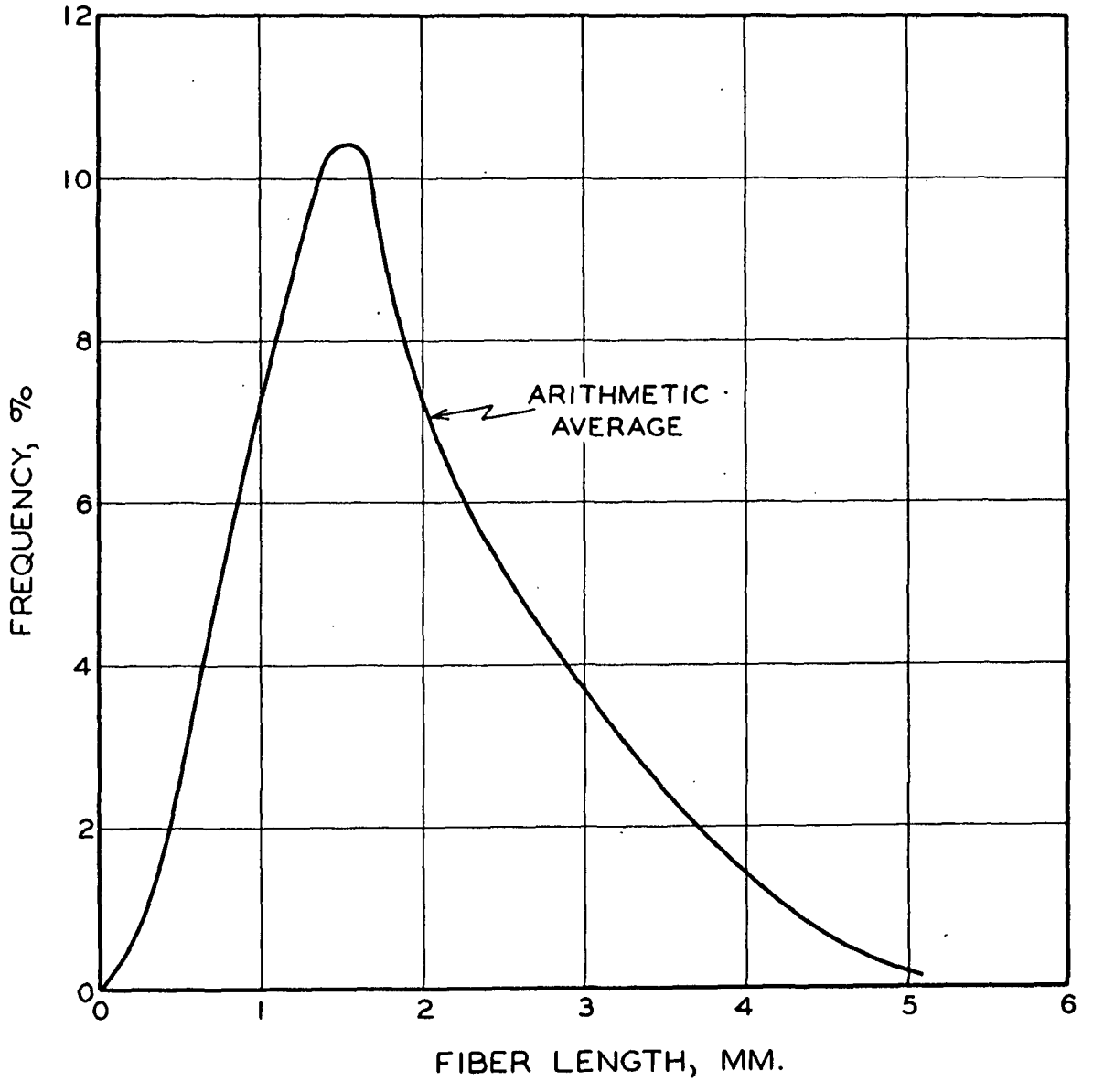

Figure 4. Fiber Length Distribution

TABLE I

FIBER DIMENSIONS AND MASS--CLASSIFIED BLEACHED SULFITE

	Maximum	Minimum	Arithmetic Average
Perimeter, microns	180	46	95
Cross-sectional area, $cm.^2$	--	--	2.90×10^{-6}
Length, mm.	5.2	0.1	2.04
Fiber mass, g.	--	--	3.61×10^{-7}
Fiber width, microns	82	17	39
Specific surface, $cm.^2/g.$ (perimeter x length/mass)			5370
Specific volume, cc./g. (area x length/mass)			1.64
Equivalent fiber thickness[a], microns ($4 \times$ area/$\pi \times$ width)			9.5
Axis ratio, width/thickness			4.1
Length-to-width ratio			52

[a] Based on assumed elliptical cross section.

cross-sectional area by assuming an elliptical fiber shape. Even in a classified wood pulp where all fine fiber debris and short fibers and fragments have been carefully removed, the results in Table I emphasize the essentially heterogeneous nature of a wood pulp fiber population.

HYDRODYNAMIC EVALUATION OF FIBER PROPERTIES

The hydraulic radius model as used in the Kozeny-Carman theory for relating porous media permeability to particle properties (5) has been widely utilized as a means of calculating particle specific surface from hydrodynamic

data. When fiber mats constitute the porous medium, the additional complications of mat deformation under fluid drag and fiber swelling must be taken into account, and over the last ten years have led to the development of a modified hydraulic radius theory (5, 6). To minimize decay effects, constant-rate filtrations of dilute slurries to form thick mats have been used to evaluate fiber properties of specific surface and specific volume in the following manner.

As shown in Appendix II, the viscous flow correlation may be rectified to yield

$$\frac{\Delta P}{c_p^{1/2}\, t} = m_1 + m_1 m_2 c_p^3 \qquad (1).$$

Thus, the modified hydraulic radius theory predicts that constant-rate filtration and mat compressibility data will yield a linear relationship when the left-hand member of Equation (1) is shown as a function of the cube of the mat density, c_p, at a compacting pressure equivalent to the over-all pressure drop, ΔP, at filtration time t. The intercept (m_1) and slope ($m_1 m_2$) of the linear correlation of the data may be used to calculate fiber specific volume, v, and fiber specific surface, S_v, (as shown in Appendix II) from

$$v = \left(\frac{m_2}{57}\right)^{1/3} \frac{1}{\left(1 - \frac{N}{2}\right)^2} \qquad (2)$$

$$S_v = \left[\frac{m_1}{\mu \rho s U^2 3.5 \left(1 - \frac{N}{2}\right) v^{3/2}}\right]^{1/2} \qquad (3).$$

Mat compression data were obtained by measuring mat density, c, as a function of mechanical compacting pressure, p_s, and correlating them according to the empirical compressibility function

$$c = Mp_s^N \qquad (4).$$

The results of four tests are shown in Fig. 5 for the classified bleached sulfite pulp. The precision of the data is excellent, and the compressibility constants M and N were determined from the linear relationship shown on logarithmic scales in Fig. 5.

The increase in pressure drop with time for duplicate constant-rate filtrations of dilute slurries to form thick mats is also shown in Fig. 5. The two runs agreed exactly, and the filtration conditions are given in Table II.

TABLE II

CONSTANT-RATE FILTRATION CONDITIONS

Pulp	Classified bleached sulfite
Filtrate velocity, U	1.80 cm./sec.
Filtrate viscosity, μ	0.827 cp. (28.5°C.)
Slurry consistency, s	0.01958%

Figure 5 is used to correlate the data according to Equation (1) by reading time and mat density at equal increments of pressure drop from 10 to 90 cm. of water. The results are shown in Fig. 6 where instead of the predicted linear relationship, the data form a slightly concave downward curve. A dashed straight line has also been fitted to the data, with the most serious deviations from linearity occurring at points corresponding to low pressure drops of 10 and 20 cm. of water.

One of the first questions to be answered in the analysis of these results is the reason for the departure from the predicted linear correlation based on the modified hydraulic radius theory. First, in one of the assumptions underlying

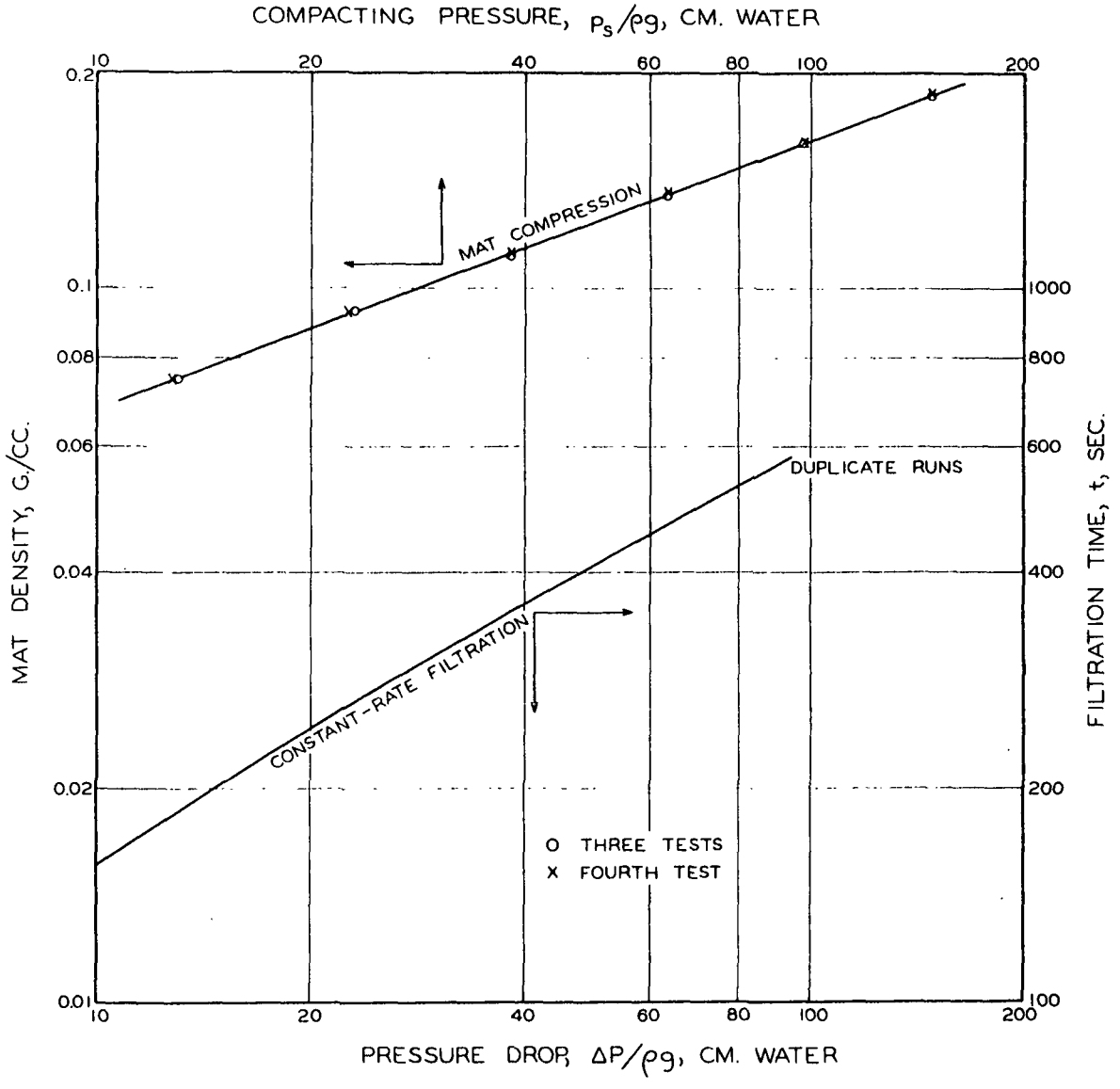

Figure 5. Constant-Rate Filtration and Compression Data

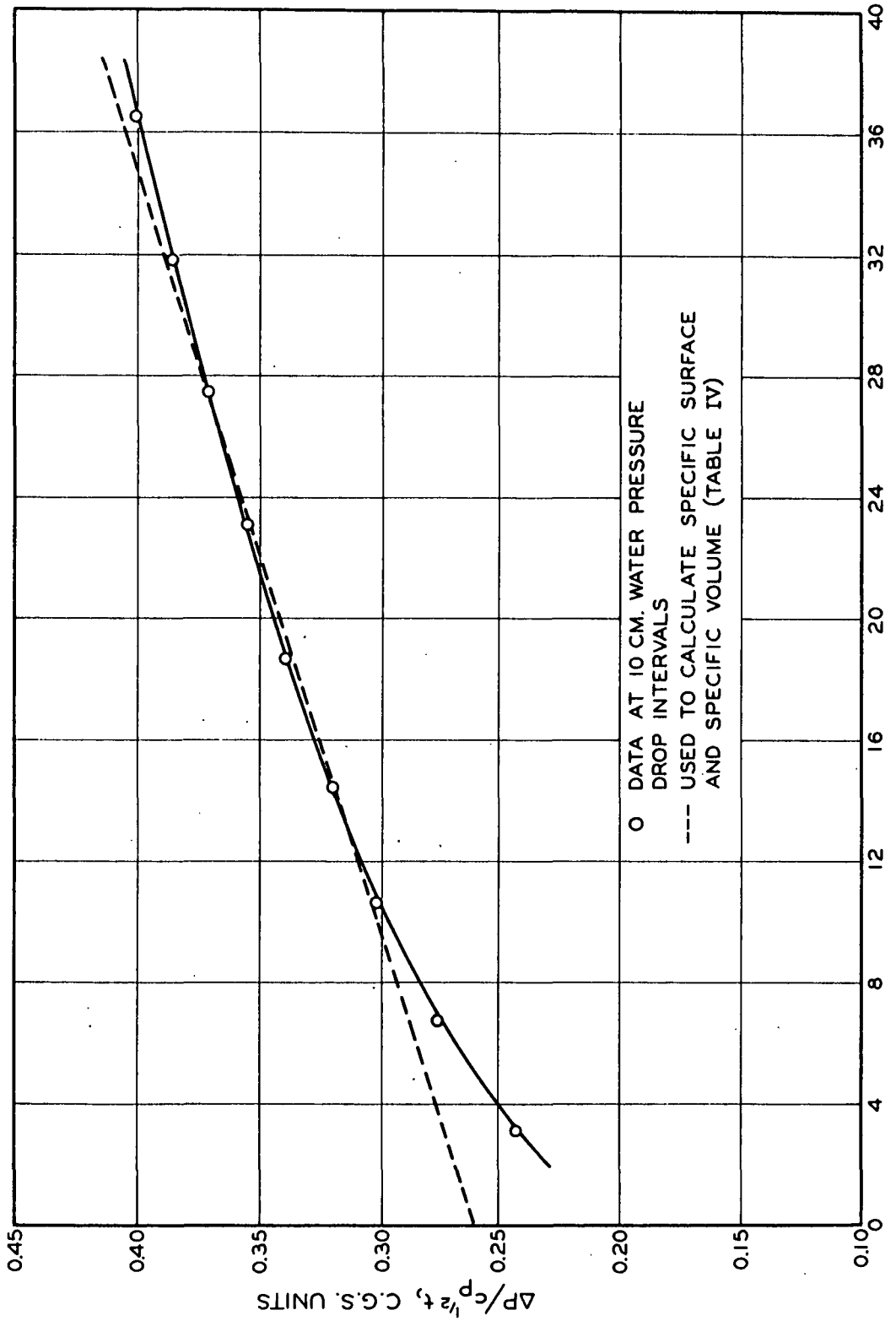

Figure 6. Rectified Equation and Data for Viscous Flow Filtration

Equation (1) certain approximations were involved in defining an average porosity. As shown in Appendix III, the modified hydraulic radius theory yields a first-order variables separable type differential flow equation which cannot be integrated analytically except for two limiting cases of (1) high porosity, and (2) a constant Kozeny factor. The integration of the differential flow equation by formula for these two limiting cases was used to define an average porosity, as shown in Appendix III, to be

$$\bar{\epsilon} = 1 - (1 - \frac{N}{2})^2 v c_p \qquad (5).$$

The definition of average porosity in Equation (5) is not completely rigorous but represents a numerical approximation. Its accuracy must be tested against the results of actual numerical integration of the differential flow equation. The porosity function in question is

$$\phi(\epsilon) = \int_0^{\Delta P} \frac{d(\Delta P)}{\frac{k(1-\epsilon)}{3.5\,\epsilon^3}} \cong \frac{\Delta P}{\frac{\bar{k}(1-\bar{\epsilon})}{3.5\,\bar{\epsilon}}} \qquad (6),$$

where $\underline{k}$, the Kozeny factor, is related to porosity by

$$k = \frac{3.5\,\epsilon^3}{(1-\epsilon)^{1/2}} [1 + 57(1-\epsilon)^3] \qquad (7).$$

In Fig. 7, a comparison is made of numerical integrations of the viscous flow porosity function $\phi(\epsilon)$ against that calculated from the average porosity defined in Equation (5) and used in Equation (6). Data are shown for three wood pulps and one synthetic fiber whose pertinent properties are listed in Table III. Over a pressure drop range in which the porosities are not less than 0.9, the porosity function calculated from numerical integration and the average porosity

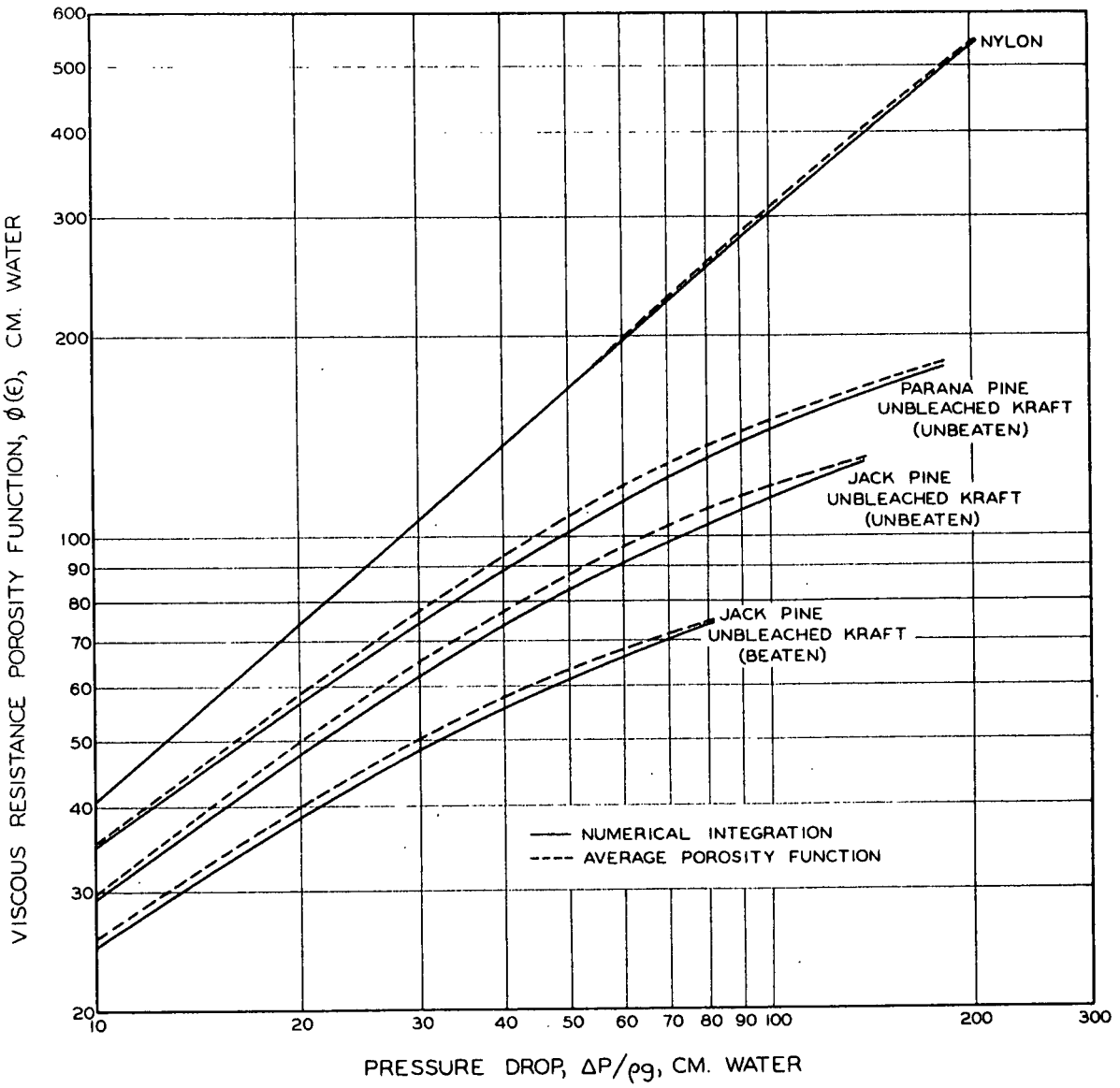

Figure 7. Comparison of Viscous Flow Porosity Function

TABLE III

FIBER PROPERTIES NECESSARY FOR CALCULATION OF VISCOUS FLOW POROSITY FUNCTION, $\phi(\epsilon)$

Fiber	Specific Volume, $\underline{v}$, cc./g.	Compressibility Constants, c.g.s. units	
		$\underline{M} \times 10^4$	$\underline{N}$
Nylon	0.904	10.70	0.225
Paraña pine (unbeaten)	3.18	9.00	0.410
Jack pine (unbeaten)	2.85	17.50	0.371
Jack pine (beaten)	3.55	17.50	0.371

function must necessarily agree, as shown in Appendix III. As the pressure drop range corresponds to porosities less than 0.9, the average porosity function gives results about 7% higher than the numerical integrations. However, the comparison of the two curves for the different fibers shows them to be of similar shape over the pressures from 10 to about 100 cm. of water. This parallel nature of the curves means that the relatively small discrepancy involved in the numerical approximation of an average porosity would not be responsible for the curvature shown in Fig. 6. In earlier work (7), the differential form of the flow equation shown in Appendix III was rectified in a form similar to Equation (1). Although the necessary slope calculations to correlate the data were not as precise as the use of the over-all pressure drop-time data as in Equation (1), curves calculated for the rectified differential flow equation showed the same type of curvature as in Fig. 6.

It may be concluded that the average porosity function for viscous flow satisfactorily represents the integrated form of the differential flow equation. The pulps represented in Fig. 7 were chosen to cover the porosity range of synthetic fibers and wood pulp fibers over wide ranges of refining and over a pressure drop range of commercial interest in sheet forming. Although either the differential flow equation or the average porosity equation may be used in the evaluation of fiber specific surface and specific volume, the use of the average porosity function is preferred because of its much greater precision.

A large number of wood pulp fibers of various species, pulped under different conditions and over wide ranges of refining levels and wide variations in fines contents, have all exhibited the same type of curvature and departure from the theoretically predicted linearity shown in Fig. 6. There appear to be three possible reasons for this lack of agreement with the modified hydraulic radius theory: (1) dependency of the Kozeny factor upon fiber shape, (2) deswelling of fibers under fluid stress with a resulting change in fiber specific volume with frictional pressure drop, and (3) dependency of fiber contact area in wet sheets upon both shape and frictional pressure drop.

In regard to the first possibility, an estimate of its importance was recently demonstrated by Bliesner (8). Bliesner prepared flattened nylon fibers of approximately elliptical shape and with an average axis ratio of about three. By using the theory of Onogi and Sasaguri (9) for estimating contact points in a bed of cylindrical fibers and Van den Akker's (10) equation for average projected area of contact in a randomly oriented sheet, and by estimating from photomicrographs the maximum possible contact area, Bliesner was able to roughly estimate the specific surface of fibers exposed to flowing water at various porosity levels.

Some of his results are summarized in Fig. 8, where the Kozeny factor for flattened nylon fibers are compared to the empirical Kozeny factor equation previously obtained for different types of cylindrical fibers (7).

If Bliesner neglects the contact area between fibers, the Kozeny factor variation with porosity calculated from water permeability measurements for the flattened nylon fibers falls only slightly below the results for cylindrical fibers. However, using Bliesner's estimate for maximum contact area, the corrected Kozeny factor curve for a flattened nylon fiber now lies considerably above the cylindrical fiber correlation. Although, admittedly, Bliesner's method of estimating contact area is necessarily crude, nevertheless it seems reasonable that the results in Fig. 8 indicate the strong possibility that the Kozeny factor for flattened fibers is significantly higher than that for cylindrical fibers. Certainly, it does not appear logical to assume a completely negligible contact area between flattened fibers of shape similar to wood pulp fibers. Thus, it may be only fortuitously true that the use of an incorrect Kozeny factor porosity function and the neglect of fiber contact area apparently counterbalance one another with the result that there is little apparent effect of fiber shape on flow resistance.

If this fortuitous counterbalancing of fiber shape and contact area effects is true for irregularly shaped wood pulp fibers, then the only remaining reason for the discrepancy between the data and the correlation predicted by the modified hydraulic radius theory in Fig. 6 is the possibility of fiber deswelling with increasing fluid stress on the fibers. It appears logical to expect that swollen wood pulp fibers would collapse to some extent at points of contact and partially lose water from the lumen and cell wall. This effect would result in a decreasing specific volume with increasing pressure drop and would give a concave

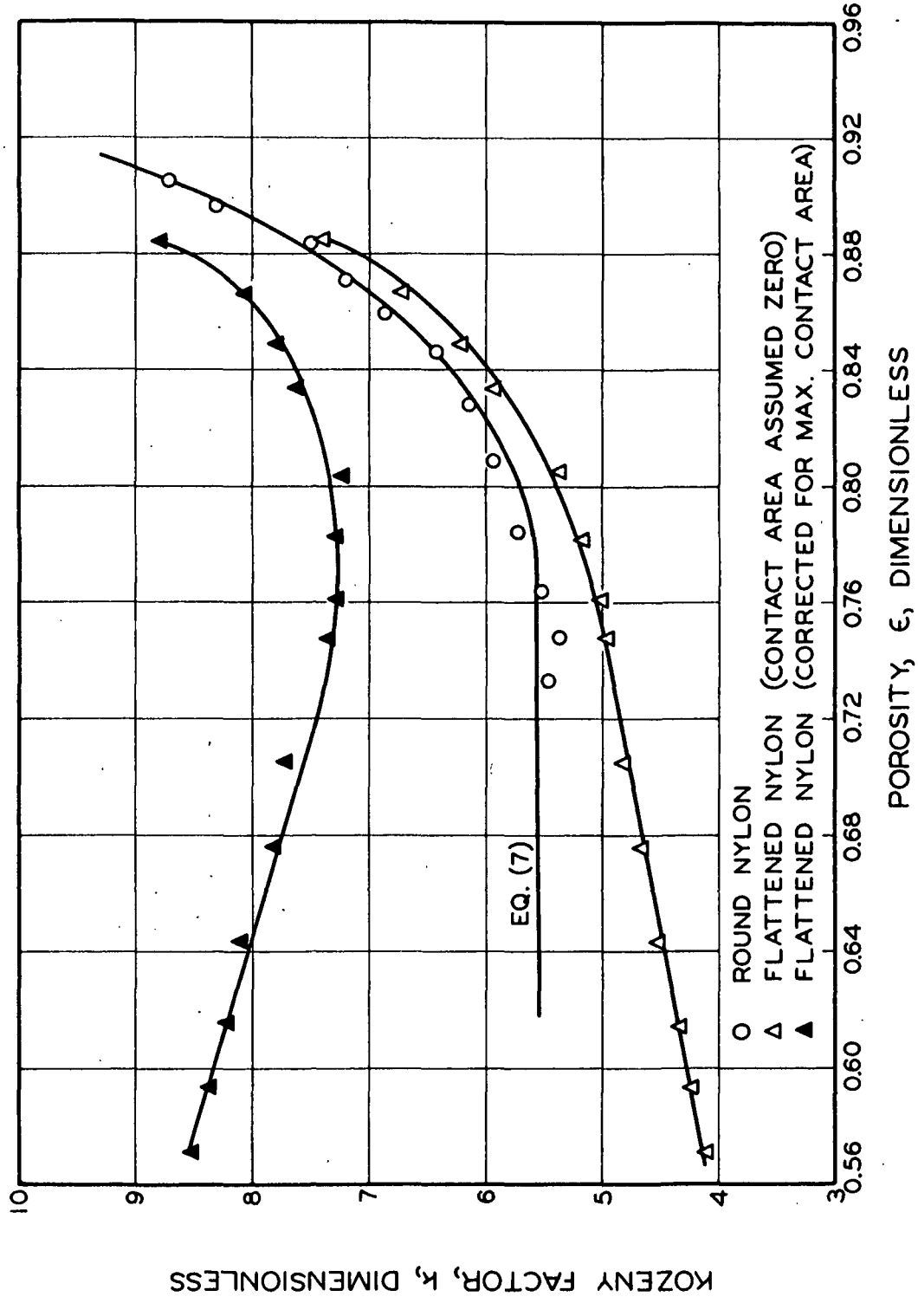

Figure 8. Bliesner's Data (8) for Kozeny Factor

downward curve of the type shown in Fig. 6. Therefore, it appears possible that the major reason for the curvature of the data is fiber deswelling and that fitting a linear relationship through the curved data points determines an average swollen specific volume over the pressure drop range represented by the data.

Because of the uncertainties of the relative contributions of fiber shape on flow resistance, changing contact area with pressure, and changing specific volume with pressure, it is impossible at this time to improve upon the flow resistance correlation represented by Equation (1). Because of severely limiting assumptions necessary in estimating the extent of these effects, improvement of the modified hydraulic radius theory must await experimental determination of these factors.

Even recognizing the above possible deficiencies in the modified hydraulic radius theory, it is easily seen from Fig. 6 that a linear relationship can be fitted to the data with only a relatively small percentage of error. For example, the maximum discrepancy of the data point representing the lowest pressure drop of 10 cm. of water is only about 10%, and the data points from 30 to 90 cm. of water do not deviate more than 1%. Therefore, for purposes of correlating hydrodynamic flow data, the use of specific surface and specific volume values calculated from the linear fit of the data would not be seriously in error provided they are utilized only over the same pressure drop range in which they are calculated.

On the basis of the linear representation of the data in Fig. 6, values of specific surface and specific volume were calculated from Equations (2) and (3), and are compared in Table IV to the previously measured microscopic values.

TABLE IV

COMPARISON OF FIBER PROPERTIES EVALUATED FROM HYDRODYNAMIC AND MICROSCOPIC MEASUREMENTS

Measurement	Specific Surface, [a] S_w, $cm.^2/g.$	Specific Volume, v, $cc./g.$	Compressibility Constants, c.g.s. units	
			M	N
Hydrodynamic [b]	5030	2.16		
Microscopic [c]	5370	1.64		
Mechanical [d]			0.00215	0.375

[a] $S_w = vS_v$.

[b] Based on data in Fig. 6.

[c] From Table I.

[d] Based on data in Fig. 5.

In view of the limitations of the two methods, the agreement in the data is considered reasonably good. The values of specific surface agree within about 5%, whereas the specific volume determined microscopically is about 25% lower than the value determined from hydrodynamic measurements. A somewhat lower value of the specific volume was anticipated from the microscopic measurements since it was not possible with the presently used cross-sectioning techniques to prepare fibers in a completely water-swollen condition. It may be concluded from the reasonably good agreement of the data in Table IV that the forcing of a theoretically predicted linear relationship to the slightly curved hydrodynamic data does not appreciably alter the physical significance of the fiber properties of specific surface and specific volume calculated from such measurements. Since we wish to use fiber

properties to predict flow behavior in this project, values of specific surface and specific volume determined hydrodynamically will be used in all subsequent calculations.

DECAY OF PERMEABILITY

Permeability measurements were made with mats whose basis weights ranged from 10 to 100 g./m.^{2} One of the immediate problems encountered in obtaining reliable data was the so-called decay of permeability effect. This was evidenced in the permeability experiments by either a gradual decrease in flow velocity at a fixed pressure drop over the mat or an increase in pressure drop over the mat with time at a given flow rate. During the first permeability studies of wood pulp, it was obvious that one of the reasons for decay of permeability was the entrapment in the mat of small amounts of impurities from the large volumes of water flowing through the mat. Elaborate precautions and procedures were used to eliminate as many impurities as possible from the water. The entire flow system was thoroughly cleaned and flushed before every trial. The water used in the 500-gal. supply tank was distilled and discarded after use if there was any indication of corrosion products from the flow system as indicated by slight mat discoloration. Water was reboiled when any evidence of dissolved air in the water system became apparent. In the limited amount of data presented in this section of the report, it was felt that decay of permeability from impurities in the water was eliminated nearly completely. Later permeation measurements had to be discarded because of an unfortunate contamination of the permeation system by a fungous growth.

The pulp used in some of the permeation studies was a classified bleached sulfite from the same source as the pulp characterized in the previous sections of this report. However, a slightly different classification procedure was used in

these studies in which only that material passing through the final 65-mesh screen in the Bauer-McNett classifier was discarded. Microscopic examination of this early classification procedure revealed some trace amounts of fines material in the pulp, and therefore in subsequent classification of the wood pulp, all the material passing through the 35-mesh screen was discarded. The examination of pulp classified in this manner indicated no visible fines or fiber debris. Because of the slight difference in early classification procedure, the hydrodynamic values of specific surface and specific volume were slightly different from those reported in Table IV. The values of specific surface and specific volume obtained for the pulp classified with this earlier procedure were 5800 $cm.^2/g.$ and 2.26 cc./g., respectively. The compressibility constants for this pulp were the same as those reported in Table IV.

When decay effects due to impurities are absent, there appear to be only three other possible reasons for decay of permeability: (1) mechanical conditioning of the mat under fluid stress because of slight oscillation of the frictional pressure drop over the mat, (2) gradual fiber deswelling at points of contact in the fiber bed, and (3) long-time creep effects because of the viscoelastic nature of cellulose. A series of permeation tests were made to determine the importance of mechanical conditioning of the bed. First, a mat of 105 $g./m.^2$ was formed in the permeation tube and pressure drop-velocity readings were taken as quickly as possible over a range of 10 to 160 cm./sec. Then when the highest velocity was reached, the velocities were very gradually decreased and the mat was allowed to expand slowly until the original velocity of about 10 cm./sec. was reached. Again, pressure drop-velocity readings were taken as quickly as possible as the velocity was increased. These cyclic measurements were repeated until there was no difference in the pressure drop-velocity data for the fiber mat.

The results of these sets of measurements are shown in Fig. 9, where it was found that after six series of cyclic measurements, the same pressure drop-velocity curve could be obtained with no decay effects apparent. About eight hours were required to carry out the six cyclic measurements, after which water was allowed to permeate at the highest flow rate for one hour. During this one-hour flow period, no decay of permeability was noted. In this type of mechanical conditioning of the mat by fluid shear stresses, it can be seen from Fig. 9 that a tremendous difference in the mat permeability can be realized. For example, at a flow rate of 10 cm./sec., the pressure drop over the mat has increased from about 20 to 90 cm. of water. The difference between the two curves in Fig. 9 represents the maximum zone of uncertainty that might be found in permeation measurements because of decay of permeability. One might imagine a mat through which a fixed velocity was to be maintained and whose permeability would be originally given by the lower curve in Fig. 9 with a minimum of decay effects. If a fixed velocity was then maintained for an infinitely long time, the decay in permeability as evidenced by the increase in pressure drop across the mat with sustained flow would be represented by the upper curve in Fig. 9.

Only a change in mat porosity could be responsible for the difference in permeability curves in Fig. 9. Mechanical compressibility measurements were made to mechanically condition a mat with the permeable piston described in the Experimental section of this report. The results of these measurements for the classified bleached sulfite pulp are shown in Fig. 10, in which the lower curve is the original first-compression curve previously given in Fig. 5. After six cycles of alternating expansion and compression of a mat of fixed basis weight, a mechanically conditioned mat was obtained, represented by the hysteresis loop of the upper solid curves. The value of the compressibility constant $\underline{N}$ has decreased from 0.375 to about 0.158 by mechanical conditioning. These compressibility constants can be

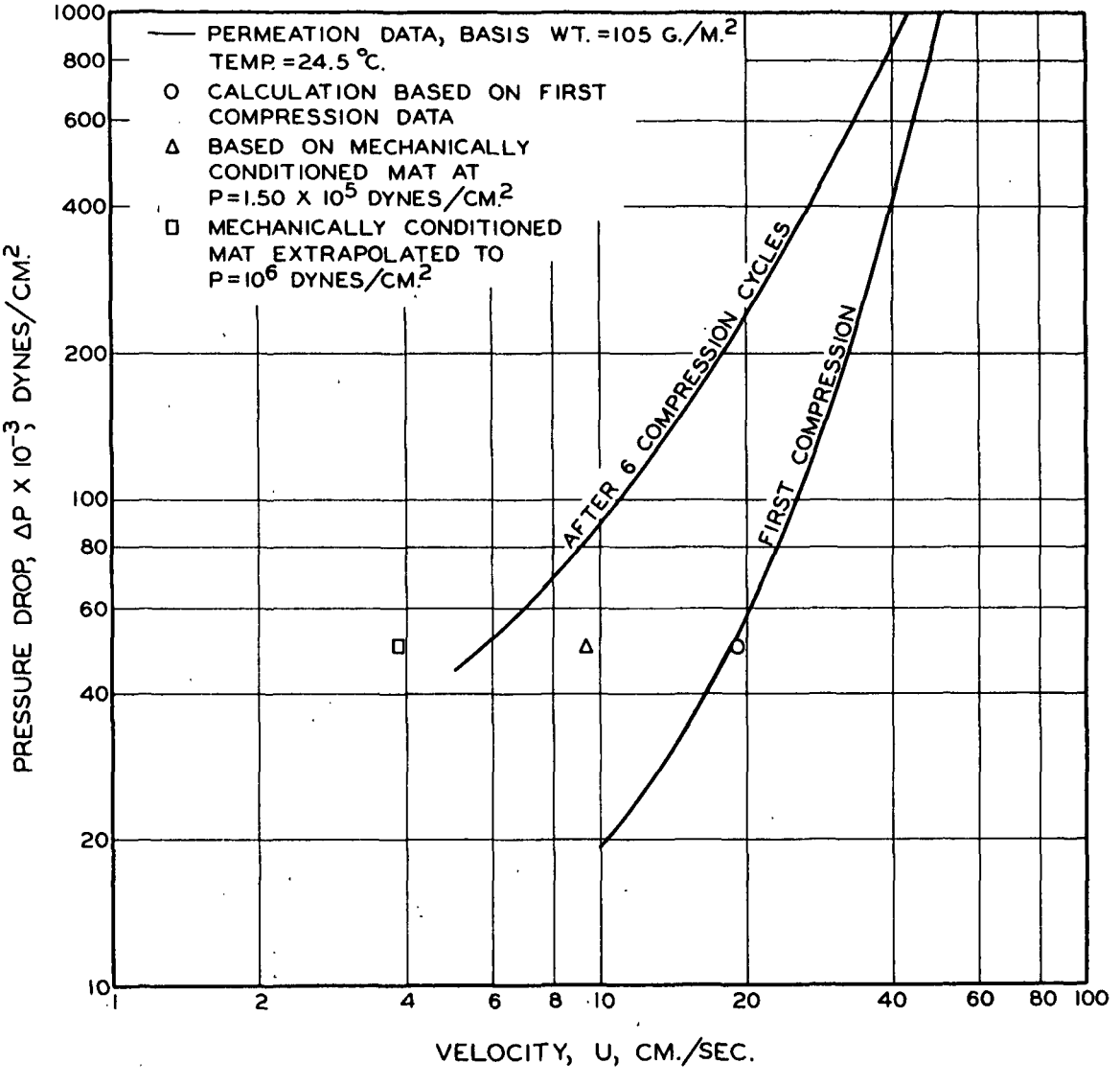

Figure 9. Decay of Permeability Phenomena

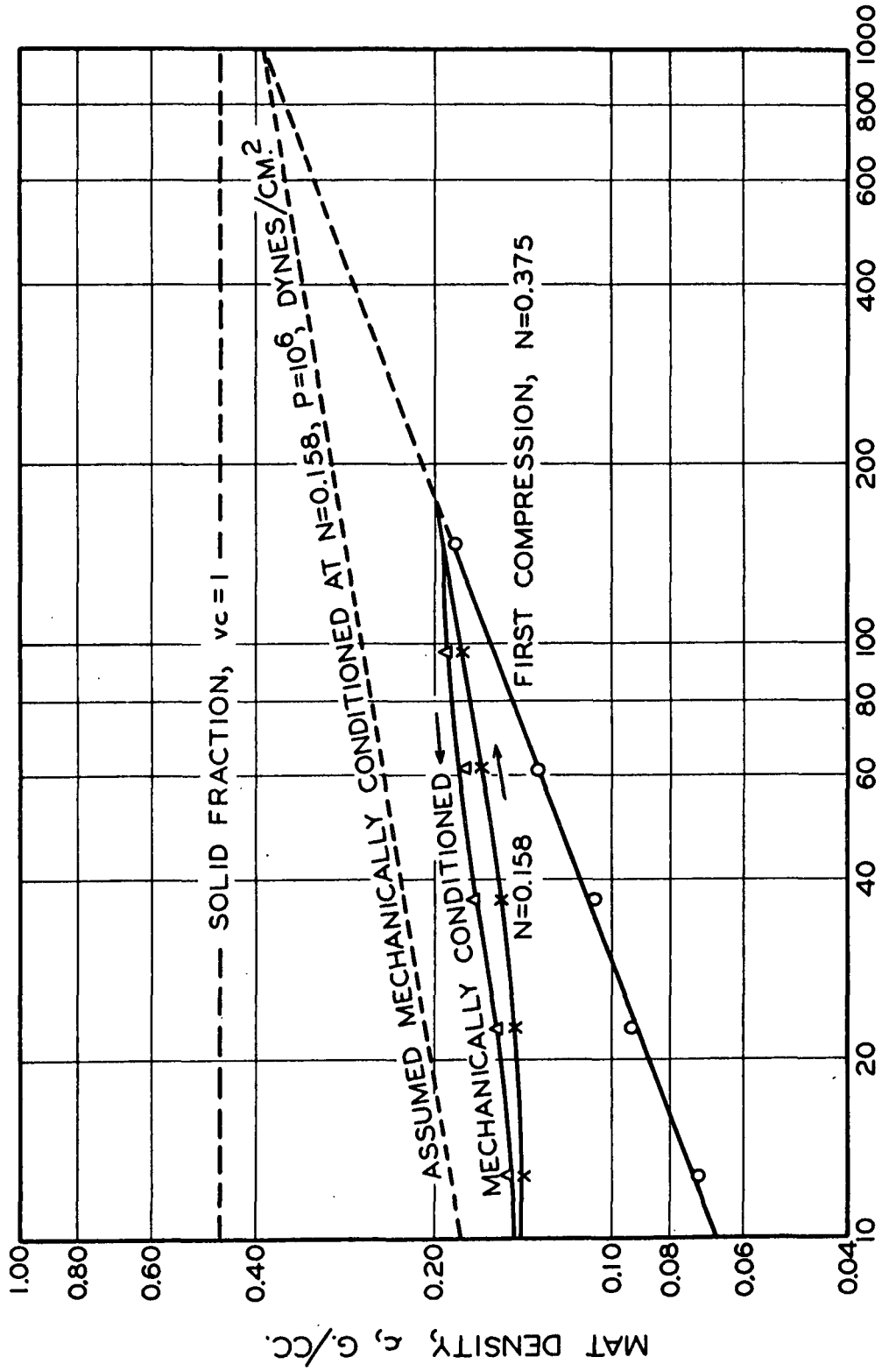

Figure 10. Mechanical Conditioning in Mat Compression

used to estimate the change in flow resistance of a mat that is mechanically conditioned by fluid stress in the following manner.

The flow relationship established previously (2, 4-6) shows the pressure gradient equivalent to the sum of a viscous and an inertial resistance such that

$$\frac{\Delta P}{W/A} = \frac{\bar{k}(1-\bar{\epsilon})}{\bar{\epsilon}^3} vS_v^2 \mu U + \frac{0.1\sqrt{\bar{k}}}{\bar{\epsilon}^3} vS_v \rho U^2 \qquad (8).$$

Using the values of the compressibility constants M and N determined for the first compression curve (Table IV), at a pressure drop of about 50 cm. of water, a predicted velocity indicated by the circular point in Fig. 9 is calculated from Equation (8). If the mechanically conditioned compression curve shown in Fig. 10 is used to estimate this effect on velocity at the same pressure drop, a point indicated by the triangle is obtained in Fig. 9 which falls roughly intermediate between the permeability curve for first fluid compression and the upper curve for a fully mechanically conditioned mat. This point represents about the minimum effect that would be expected since the upper pressure limit fixed by the mechanical compression apparatus used in obtaining the data in Fig. 10 was only about 150 cm. of water, whereas the permeation curves in Fig. 9 had a maximum pressure drop of about 2000 cm. of water. If we try to estimate the maximum effect on the mat permeation curve from the assumed dotted-line compression curve in Fig. 10 extrapolated to about 10^6 cm. of water and with the same slope as that obtained for the mechanically conditioned mat, a datum point represented by the rectangle is obtained from Equation (8) and shown in Fig. 9. This datum point falls above the permeation curve for a mechanically conditiond mat in Fig. 9.

These calculations indicate that the decrease in mat permeability by mechanically conditioning the mat with fluid stress can be explained and accounted for entirely by changes in mat compression under the cyclical action of compacting

pressure. To predict precisely the effect of mechanical conditioning on flow would require actual compression data extending to a pressure equal to the highest pressure drop of the flow measurements. The accuracy of the extrapolated or assumed compression curves in Fig. 10 cannot be relied upon. Meaningful compression data at pressures appreciably higher than those used in this study probably cannot be obtained since a solid fraction of unity is being approached. The very large mat solid fractions at high pressures would make the internal resistance of the mat to flow so large that the mat compression would become strongly time dependent. At high pressures, fiber collapse must begin to become a significant part of the mat compression, and the compressibility constants M and N would begin to vary significantly.

When a mat is subjected to fluid stress by flowing water through it either in a permeation experiment or in forming a mat in filtration, cyclical variations in frictional pressure drop will be observed because of the pump supplying water or fiber suspension. This variation in pressure may significantly alter the manner in which a mat compresses. In the previous chapter on compression (11), one example was given as to how vibration may influence the compression curve. Vibrations or frictional pressure drop fluctuations will affect the frictional forces between the points of contact of fibers in a compacted mat and thus affect the apparent density and over-all compacting pressure relationship. Decay of permeability was not a serious problem in the previous studies of synthetic fibers because of the less compressible nature of these materials as compared to wood pulp fibers.

The first fluid compression curve of wood pulp fibers has always exhibited some decay. Thus, permeation tests in which it is necessary to flow water through mats of fixed basis weights for considerably long periods of time to obtain

frictional pressure drop-velocity data will always be somewhat obscure in their interpretation because of decay of permeability phenomena.

PERMEATION AT FIXED BASIS WEIGHTS

Bearing in mind the limitations imposed by decay of permeability, a series of permeation experiments were made on classified wood fibers whose specific surface was 5800 $cm.^2/g.$, specific volume 2.26 cc./g., and compressibility constants the same as in Table IV. Six basis weights were studied from about 14 to 100 $g./m.^2$, and the experimental results are shown in Fig. 11. To obtain the data for each basis weight required a total time of about one hour of water permeation. Even though this time was kept as short as practicably possible, some decay of permeability unavoidably occurred. The experimental curves are compared to those theoretically predicted by use of the average porosity flow correlation including viscous and inertial resistance [Equation (8)]. At frictional pressure drops up to about 150 cm. of water, the experimental and theoretical curves agree within about 15% down to basis weights of about 60 $g./m.^2$ At lower basis weights, the discrepancies become larger, and at the lowest basis weights the deviations are much greater than those previously found for synthetic fibers, indicating more severe "fiber-wire interaction" phenomena (2).

To determine the reason for the discrepancies, it is first necessary to test the use of the average porosity flow correlation including the inertial resistance term. Previously, it was shown in Fig. 7 that the viscous resistance average porosity function agreed well with that calculated from exact numerical integration. When the inertial term is included in the integration of the differential flow equation, the porosity terms cannot be separated from the flow velocity, and the validity of the average porosity concept must be tested at various flow velocities. The flow equation was numerically integrated as shown in

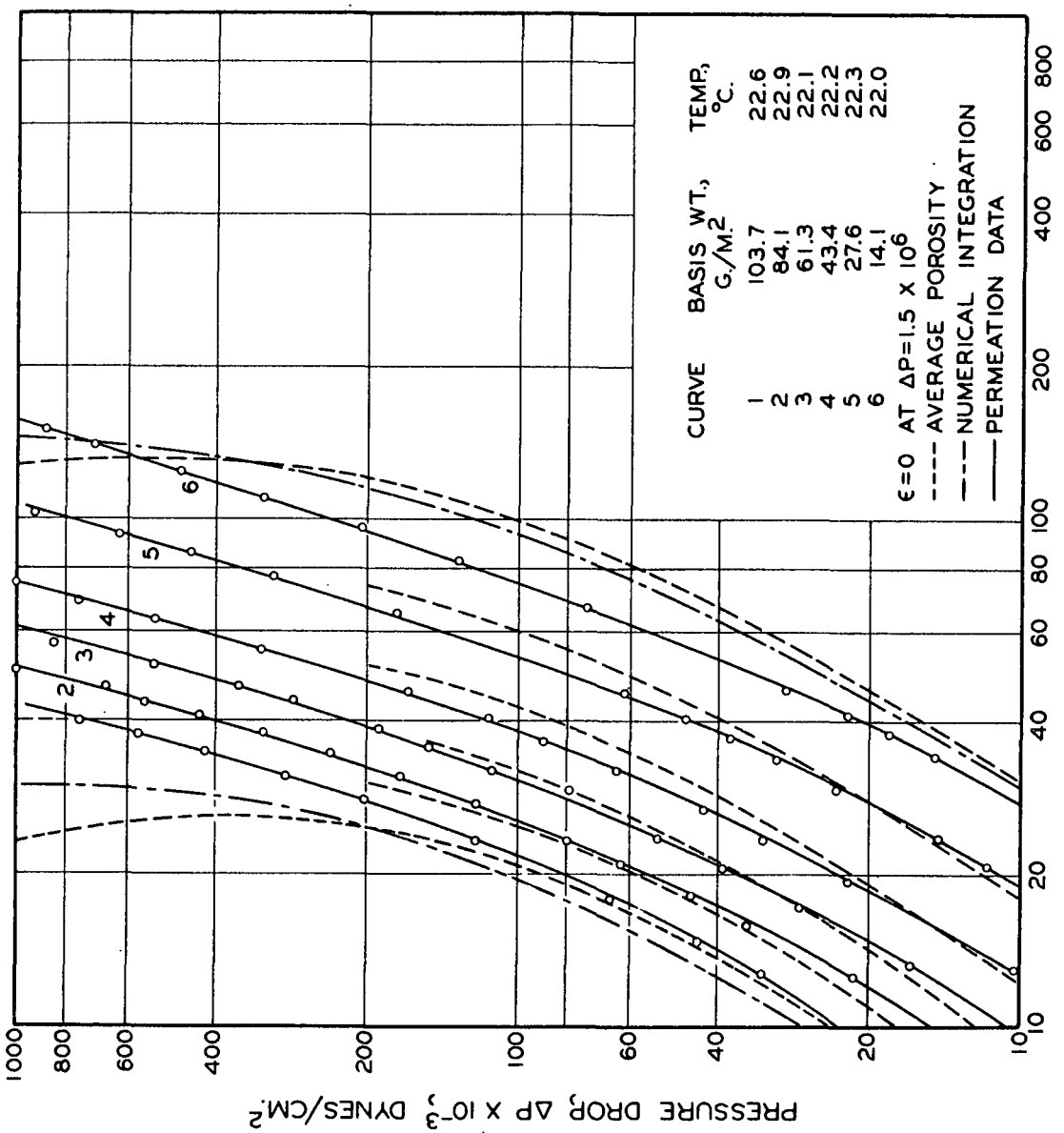

Figure 11. Permeation Data and Calculated Results

Appendix IV and with the aid of a digital computer. The results of a series of two numerical integrations at a high and a low basis weight representing different velocity regions are compared to the results calculated from the average porosity relationship and are shown in Fig. 11. It is seen that up to pressures of about 150 cm. of water the curves calculated from the average porosity integration and by numerical integration are very nearly parallel to one another. At a fixed pressure drop the calculated velocities differ by less than 10%. Because the curves are parallel and because the values of specific surface and specific volume are themselves determined from the average porosity equation with the viscous flow term, it may be concluded that the use of an average porosity relationship is justified in the flow equation including inertial resistance up to pressure drops of about 150 to 200 cm. of water. The minimum mat porosity at the forming wire at 200 cm. of water for most wood pulp fibers would be about 0.6.

At pressure above 150 cm. of water, the average porosity correlation calculations show that a maximum velocity is reached at a fixed basis weight and then greater frictional pressure drops produce lower velocities. Physically, this calculated maximum in velocity is not possible to achieve, and the average porosity relationship is not valid at pressure drops beyond about 150 cm. of water. The results predicted by numerical integration show that at pressure drops over 150 cm. of water the pressure drop increases extremely rapidly with increased flow rate. This is because at a pressure drop of 1.5×10^6 dynes/cm.^{2} the mat porosity at the wire would become equal to zero and no more flow would be physically possible. The numerically integrated flow equation should be valid for porosities approaching zero provided that the fiber specific volume does not decrease because of fiber deswelling at points of contact under the influence of extremely high pressures. The experimental data do not show the predicted rapid increase in pressure drop

with increased velocity at pressure drops greater than 150 cm. of water. It is speculated that the reason for this is an actual decrease in swollen specific volume of fibers at high pressures with the result that the measured pressure drops are lower than those predicted by assuming the specific volume stays constant. This deswelling may also be accompanied by a decrease in mat compressibility. Because of this apparent deswelling of fibers at high pressures and low porosities, use of the flow correlation with an assumed constant specific volume is not justified at pressures appreciably greater than 150 cm. of water. Thus, in Fig. 11, the calculated curves for most of the basis weights are not shown beyond this point.

The permeation experiments have shown reasonable agreement with the flow correlation at basis weights greater than about 60 g./m.^{2} and at pressure drops up to about 150 cm. of water. At higher pressure drops the data show that the pressure drop does not increase as rapidly at increasing velocities as predicted because of a significant fiber deswelling at higher pressure drops. At lower basis weights the flow correlation shows a very significant fiber-wire interaction with the result that the measured pressure drops at a given velocity may be as great as twice that predicted from the flow correlation at a given velocity. However, because of the presence of some decay effects and because of the difficulty of eliminating severe decay effects because of impurities in the water system, permeation experiments were abandoned at this point in the work and subsequent data were obtained in the dynamic drainage tester.

DYNAMIC DRAINAGE AT CONSTANT VELOCITIES

A series of tests were made in the dynamic drainage tester with the classified bleached sulfite pulp characterized in Table IV. The primary data obtained are frictional pressure drop versus sheet-forming time at a constant

velocity of flow. Flow velocities from about 1 to 100 cm./sec. can be studied. The primary data of frictional pressure drop *versus* forming time can be transformed to pressure drop *versus* mat basis weight by a simplified form of the material balance for dilute slurries and complete fiber retention (Appendix II) in which

$$\frac{W}{A} = \rho s U t \qquad (9)$$

where s is the slurry consistency and t is the forming time at constant drainage velocity, U.

To check the reproducibility of the data for the wood pulps, five runs were made for each of five velocities from about 20-40 cm./sec. Several runs were made at higher velocities of from about 50-100 cm. of water. The run conditions are summarized in Table V. The reproducibility of the data is indicated by comparing the experimental pressure drops at a fixed filtration time corresponding to the attainment of a predicted frictional pressure drop of 30×10^3 dynes/cm.^{2} The reproducibility of the data are good, as seen by the average deviations from the mean of about 3 to 8%. The variations that do occur from run to run are mainly because of minor temperature variations and small errors involved in the accurate determination of velocity (the calculation of a filtration-time curve involves a cubic equation in velocity and small errors in determination of velocity tend to be magnified). It can also be seen from Table V by comparing the experimental and and predicted pressure drops at a given filtration time corresponding to the predicted pressure drop of 30×10^3 dynes/cm.^{2} that the discrepancy between the experimental and predicted results increase with increasing velocities. It will be shown that this effect is due primarily to a fiber-wire interaction phenomenon related to basis weight rather than velocity.

TABLE V

DYNAMIC DRAINAGE TESTS

Run No.	Consistency, $\underline{s}$, g./cc. x 10^4	Temp., °C.	Velocity, $\underline{U}$, cm./sec.	Exp. Pressure Drop, $\Delta\underline{P}_e \times 10^{-3}$, dynes/cm.^{2} [a]	Deviation from Mean, %	$\Delta\underline{P}_e/30 \times 10^3$
A-1	0.889	23.5	20.1	32.0	5.0	1.06
B-1	0.889	24.0	19.9	34.0	0.9	1.13
C-1	0.928	24.5	19.8	33.7	0.0	1.12
D-1	0.947	26.3	20.1	32.2	4.5	1.07
E-1	0.913	24.0	19.8	36.8	9.2	1.23
			Av.: 19.9	33.7	3.9	1.12
A-2	0.900	23.5	24.4	33.0	3.8	1.10
B-2	0.915	24.0	26.0	34.1	0.6	1.14
C-2	0.955	24.5	25.1	33.6	2.0	1.10
D-2	0.956	26.3	24.8	36.4	6.1	1.21
E-2	0.955	24.0	24.9	34.5	0.6	1.20
			Av.: 25.0	34.3	2.6	1.15
A-3	0.899	23.5	30.2	35.0	0.9	1.17
B-3	0.934	24.0	30.0	33.6	3.2	1.12
C-3	0.972	24.5	30.2	31.5	9.2	1.05
D-3	0.950	26.3	30.2	36.9	6.4	1.23
E-3	0.935	24.0	30.2	35.5	2.3	1.18
			Av.: 30.2	34.7	4.4	1.15
A-4	0.895	23.5	34.6	32.8	13.2	1.09
B-4	0.930	24.0	34.8	36.4	3.7	1.21
C-4	0.955	24.5	34.9	36.6	3.2	1.21
D-4	0.933	26.3	35.0	44.1	16.7	1.47
E-4	0.933	24.0	34.9	39.8	5.3	1.32
			Av.: 34.8	37.8	8.4	1.26
A-5	0.917	23.5	39.6	34.5	8.3	1.15
B-5	0.921	24.0	39.5	34.5	8.3	1.15
C-5	0.944	24.5	39.9	39.0	0.8	1.30
D-5	0.914	26.3	39.7	40.5	4.6	1.35
E-5	0.927	24.0	40.0	45.2	16.8	1.50
			Av.: 39.7	38.7	7.8	1.29
F-1	0.389	24.5	49.9	--	--	--
G-1	0.393	25.8	49.4	--	--	--
F-2	0.389	24.5	64.5	60.0		2.00
G-2	0.396	26.0	65.0			
H-2	0.418	25.8	64.9			
F-3	0.380	24.5	79.5	62.0		2.07
G-3	0.397	26.0	81.0			
H-3	0.406	25.8	80.0			
F-4	0.382	24.5	99.3	77.5		2.58
G-4	0.390	26.0	100.9			
H-4	0.392	25.8	102.6			

[a] $\Delta\underline{P}_e$ is the actual pressure drop at a filtration time corresponding to a predicted pressure drop of 30×10^3 dynes/cm.^{2}

An example of one of the recorded pressure traces is given in Appendix V together with sample calculations for translating the results of pressure-time curves to pressure-basis weight curves. The results of a set of runs (the "A" and "F" runs from Table V) over the entire velocity range are shown in Fig. 12 and 13 for low and high velocity ranges, respectively.

The predicted pressure drop-time curves shown in these figures were conveniently obtained by tracing on the x-y plotter of an analog computer. The procedure used in the analog computer solution of the differential flow equation is given in Appendix VI. The results show that at a given filtration time the experimentally measured pressure drops are consistently higher than the predicted flow correlation, the discrepancy becoming worse at higher velocities. The data from Fig. 12 and 13 have been transformed into pressure drop-basis weight curves in Fig. 14. It can be seen that because of the lower slurry consistencies used in the higher velocity range data, the runs cover basis weights up to only about 30 g./m.^{2}, whereas the lower range velocity data extend up to basis weights of about 70 g./m.^{2}

First, to check on the possibility that slightly different values of fiber properties determined in viscous flow or a slightly different value of a coefficient of inertial resistance from that previously estimated from a study of synthetic fibers (2, 4) may have been responsible for the observed discrepancies between the experimental and predicted results, the flow correlation was tested in the following manner. The differential form of the flow correlation may be written in a rectified form as (Appendix V):

$$\frac{1}{U}\,\frac{d(\Delta P)}{d(W/A)} = a + bU^2 \qquad (10),$$

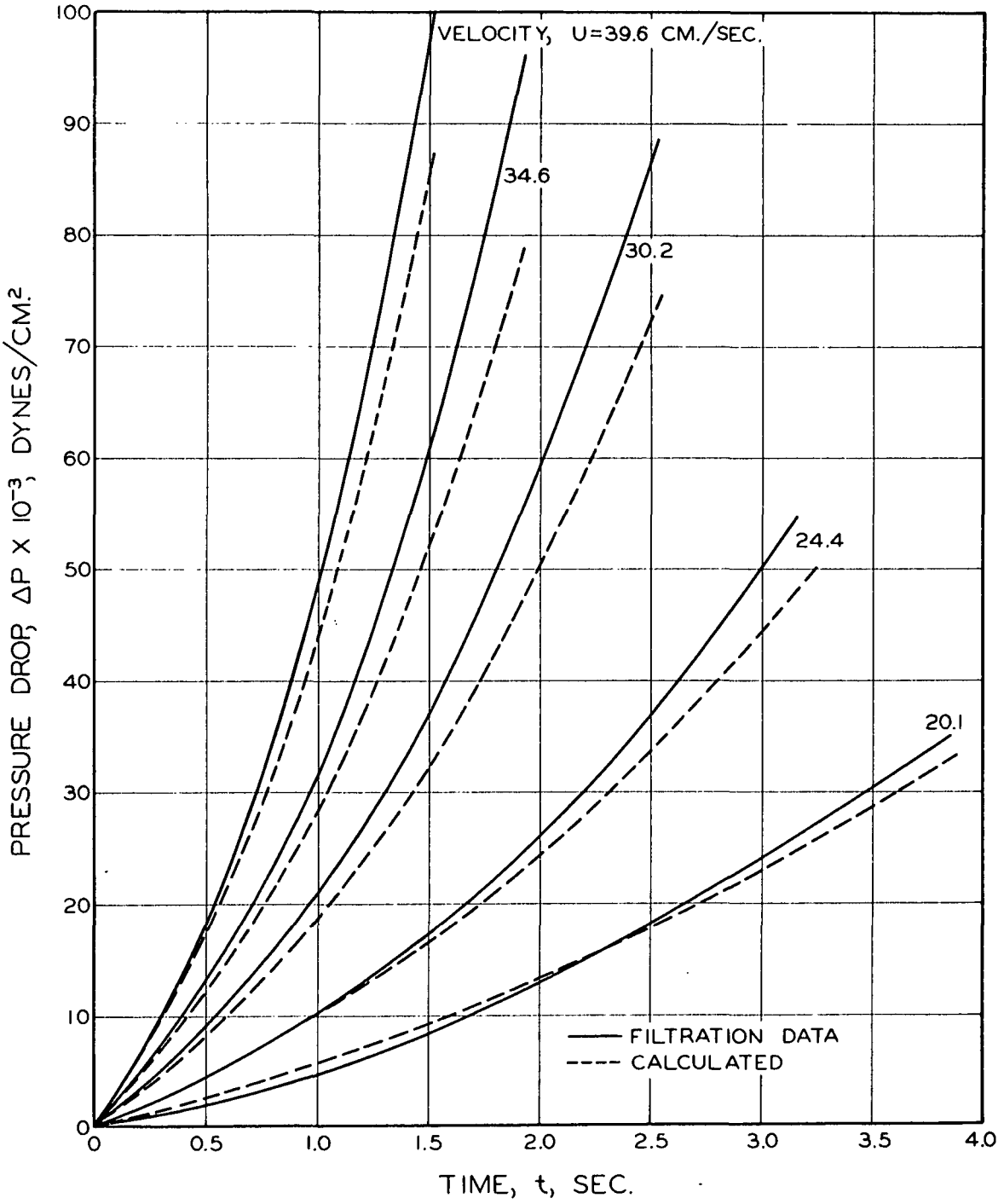

Figure 12. Dynamic Drainage Tester Data--Low-Velocity Range

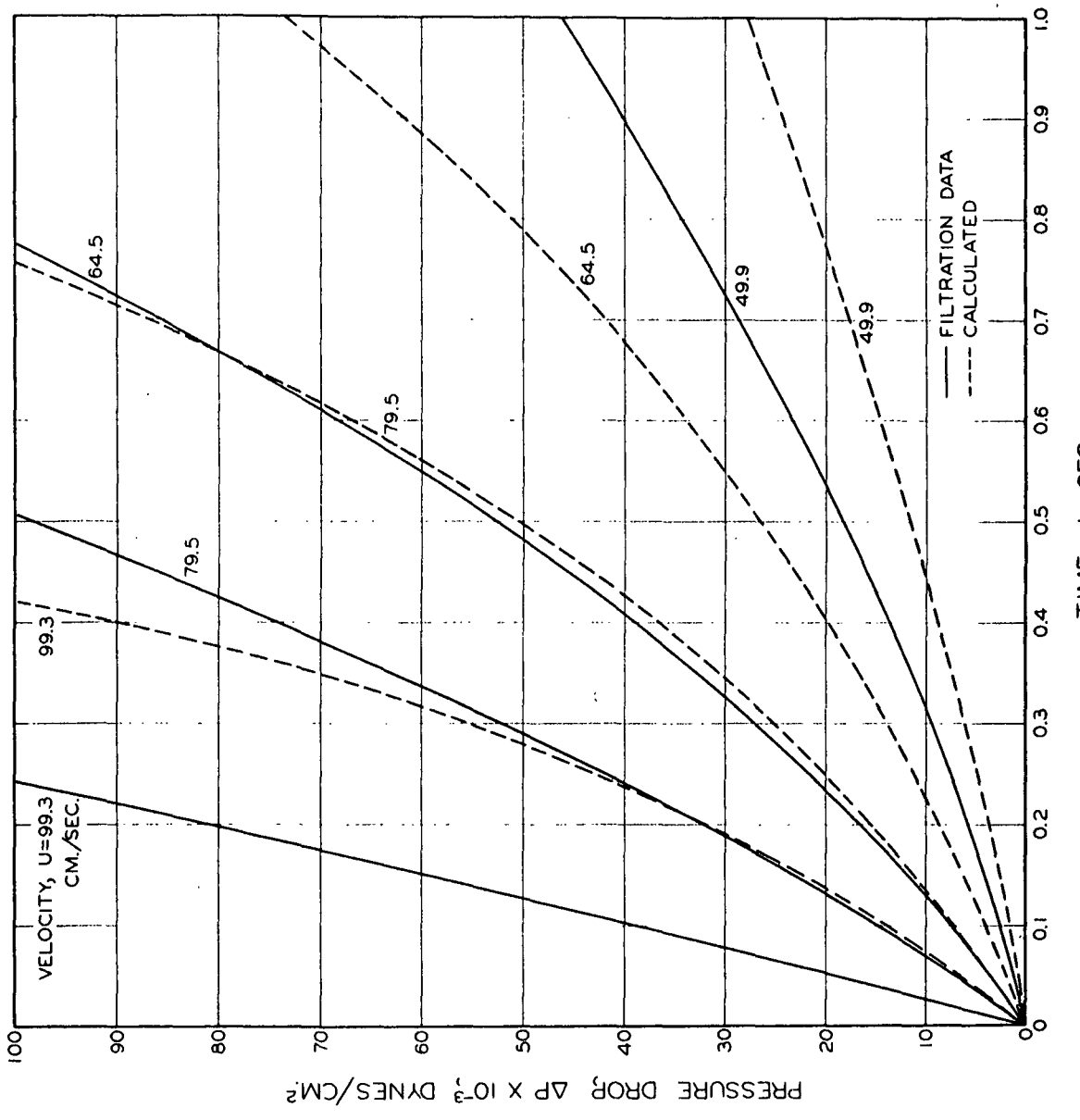

Figure 13. Dynamic Drainage Tester Data--High-Velocity Range

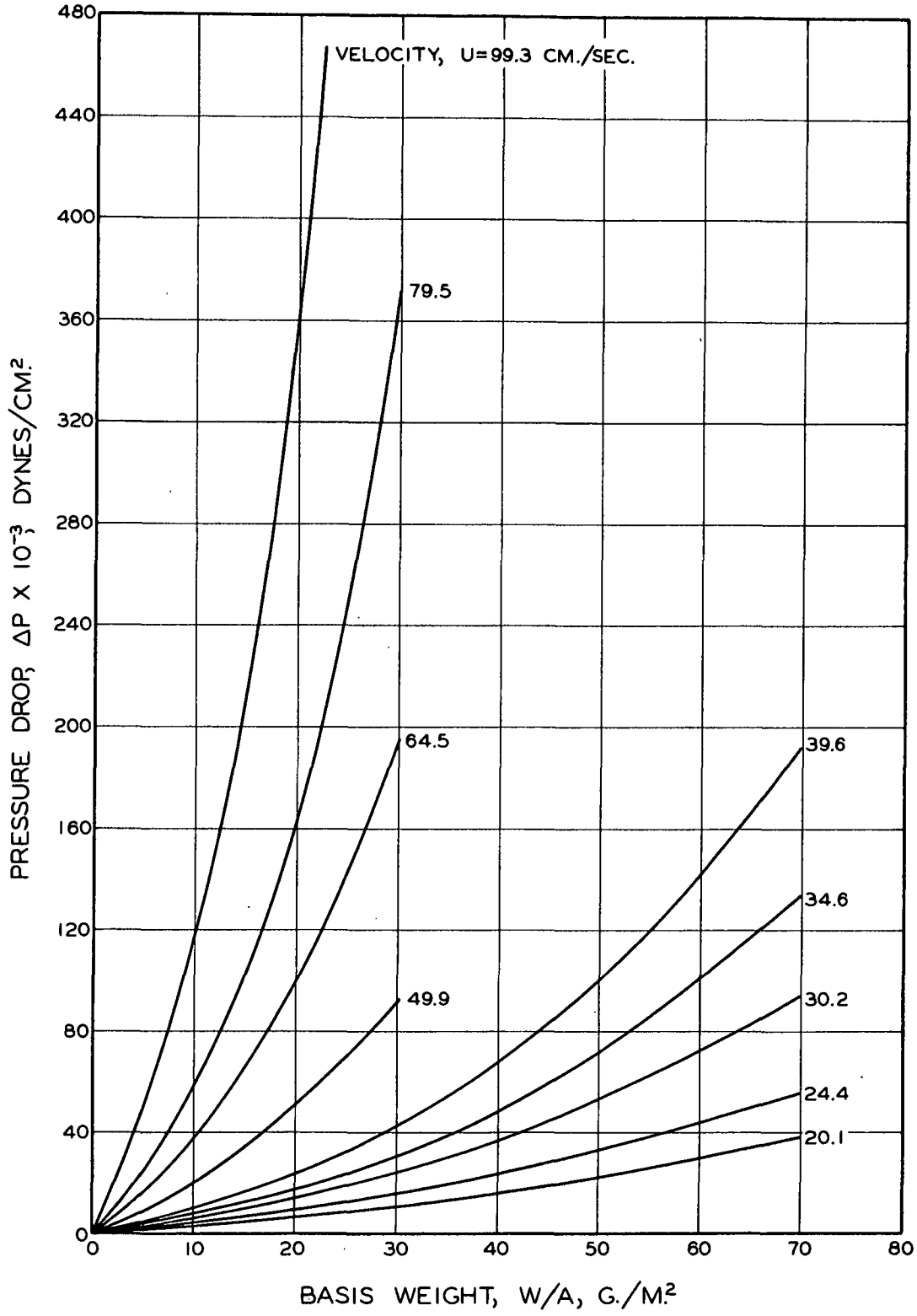

Figure 14. Frictional Pressure Drop for Constant-Rate Mat Formation

where

$$a = \frac{k(1 - \epsilon)}{\epsilon^3} vS_v^2 \mu \qquad (11),$$

$$b = \frac{b'\sqrt{k}}{\epsilon^3} vS_v \rho \qquad (12),$$

b' = coefficient of inertial resistance, equals 0.1 for cylindrical fibers of uniform diameter (2, 4).

If the left-hand member of Equation (10) at arbitrarily selected constant pressure drops is shown as a function of velocity, a linear relationship should be obtained since the terms a and b should be functions only of pressure drop, provided Equation (10) is valid. The results of such a method of interpreting the data are shown in Fig. 15, where a definite curvature of the constant-pressure plots is seen, indicating the general failure of the flow correlation.

The previously discussed permeation data at constant mat basis weights indicated the possibility of fiber-wire interaction at low basis weights. To isolate this supposed basis weight effect, the data from Fig. 14 were cross plotted at arbitrarily selected constant values of basis weight, and are shown in Fig. 16. In addition, photomicrographs of the fiber deposits on the 100-mesh screen over the same basis weight range of the data shown in Fig. 16 are shown in Fig. 17-19. Figure 20 shows the water-saturated fibers themselves at a higher magnification. In Fig. 17, at a basis weight of 12.1 g./m.^{2}, it can be seen that the formed mat has an equivalent thickness of only 2-3 fibers. As discussed in the analysis of synthetic fiber data in Report Two (2), such a mat cannot be presumed to have a porosity distribution equivalent to that of a much thicker mat under the same flow conditions. In such thin structures, it is indeed more logical to assume that the average porosity given in Equation (5) approaches a more uniform porosity wherein the integrating factor $[1 - (N/2)^2]$ approaches a value of unity at zero basis

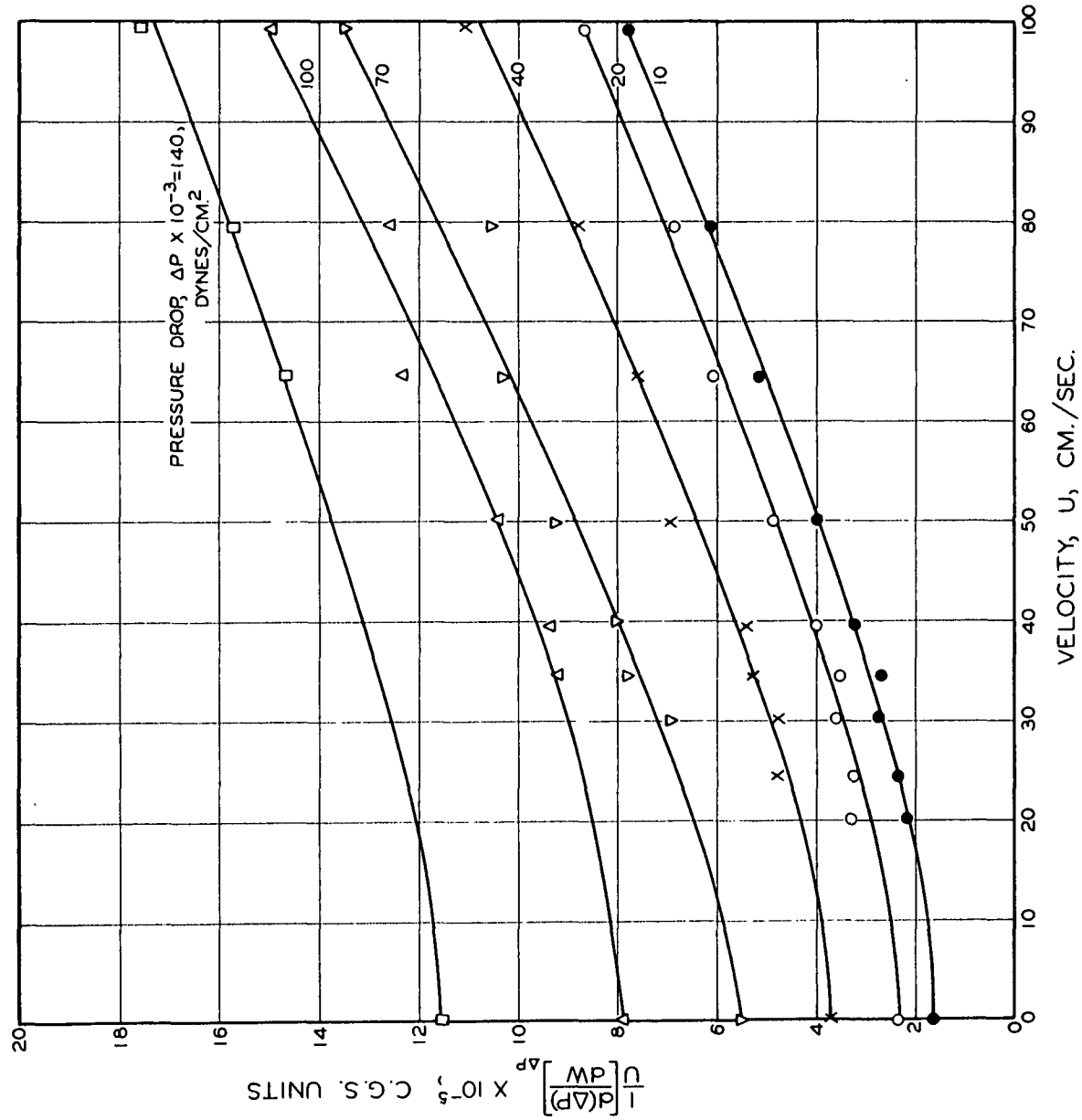

Figure 15. Rectified Form of Flow Correlation for Dynamic Drainage Tester Data

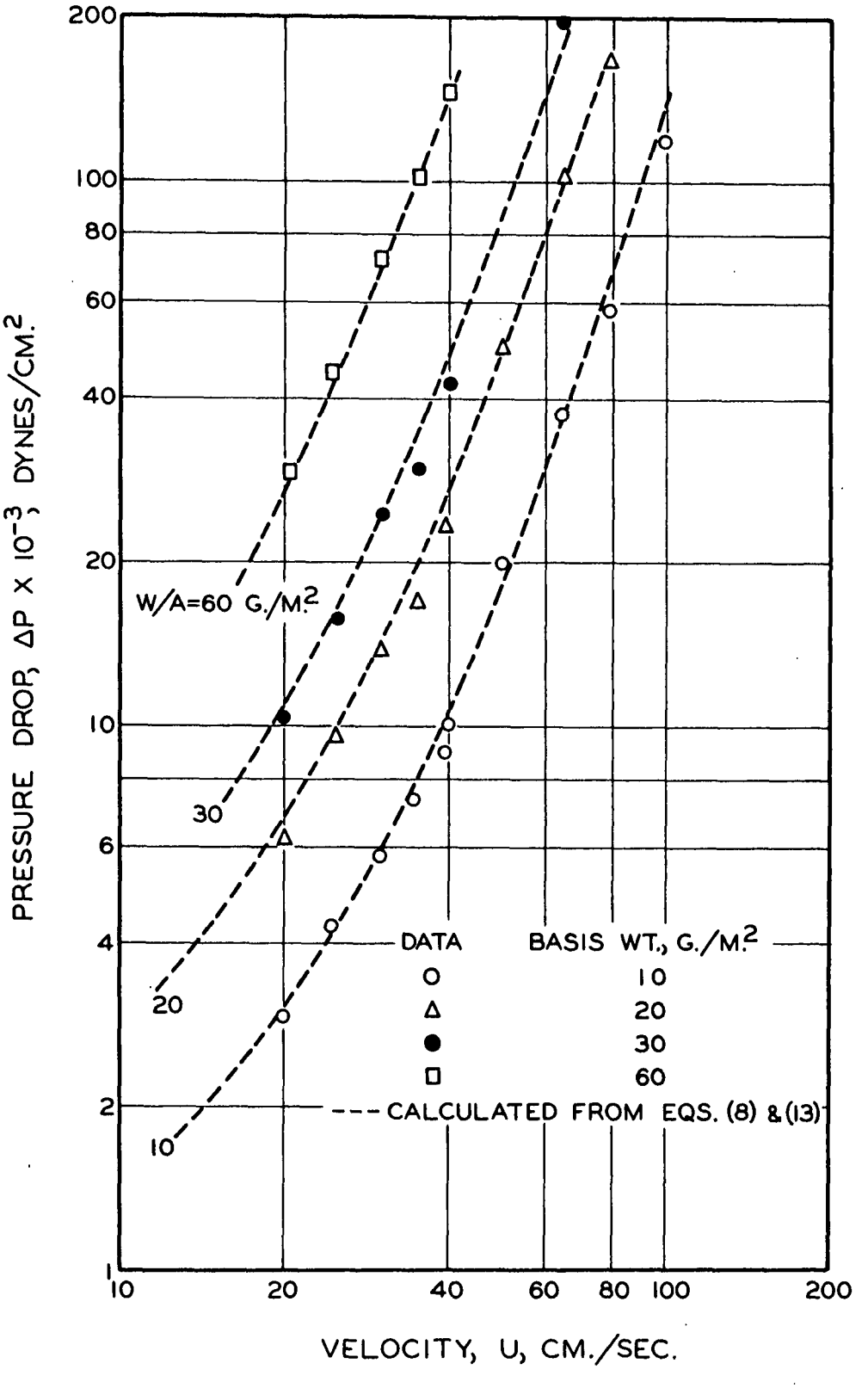

Figure 16. Pressure Drop as a Function of Velocity for Dynamic Drainage Tester Data

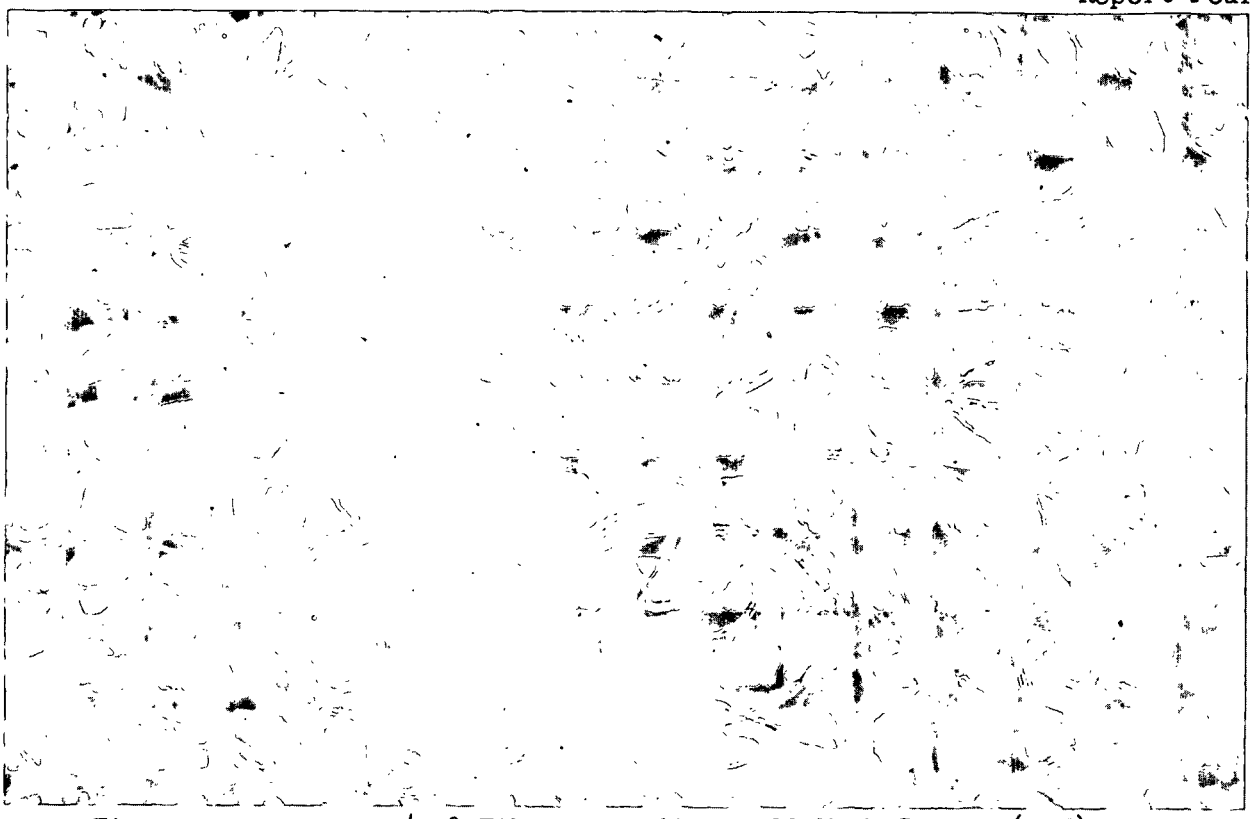

Figure 17. 12.1 g./m.^{2} Fiber Deposit on 100-Mesh Screen (40X)

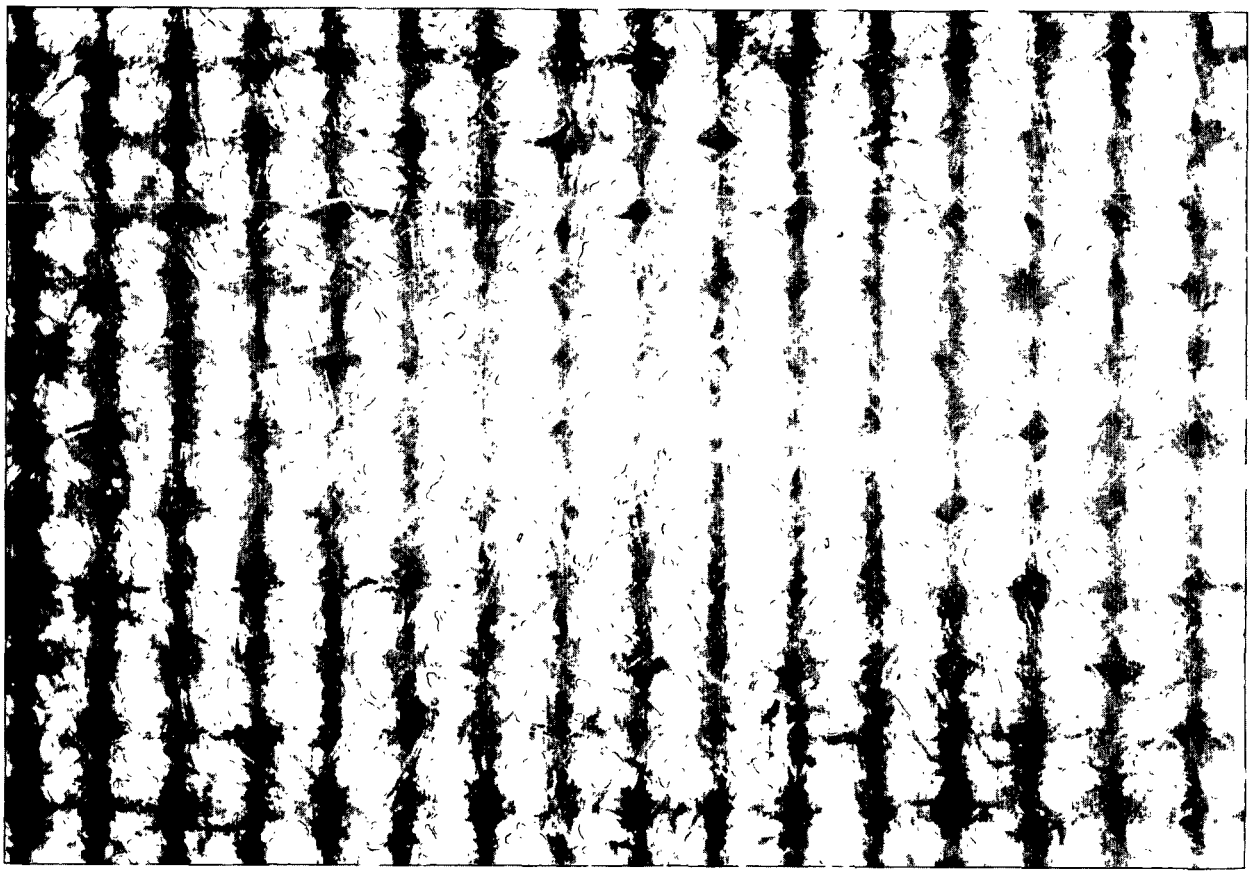

Figure 18. 37.7 g./m.^{2} Fiber Deposit on 100-Mesh Screen (40X)

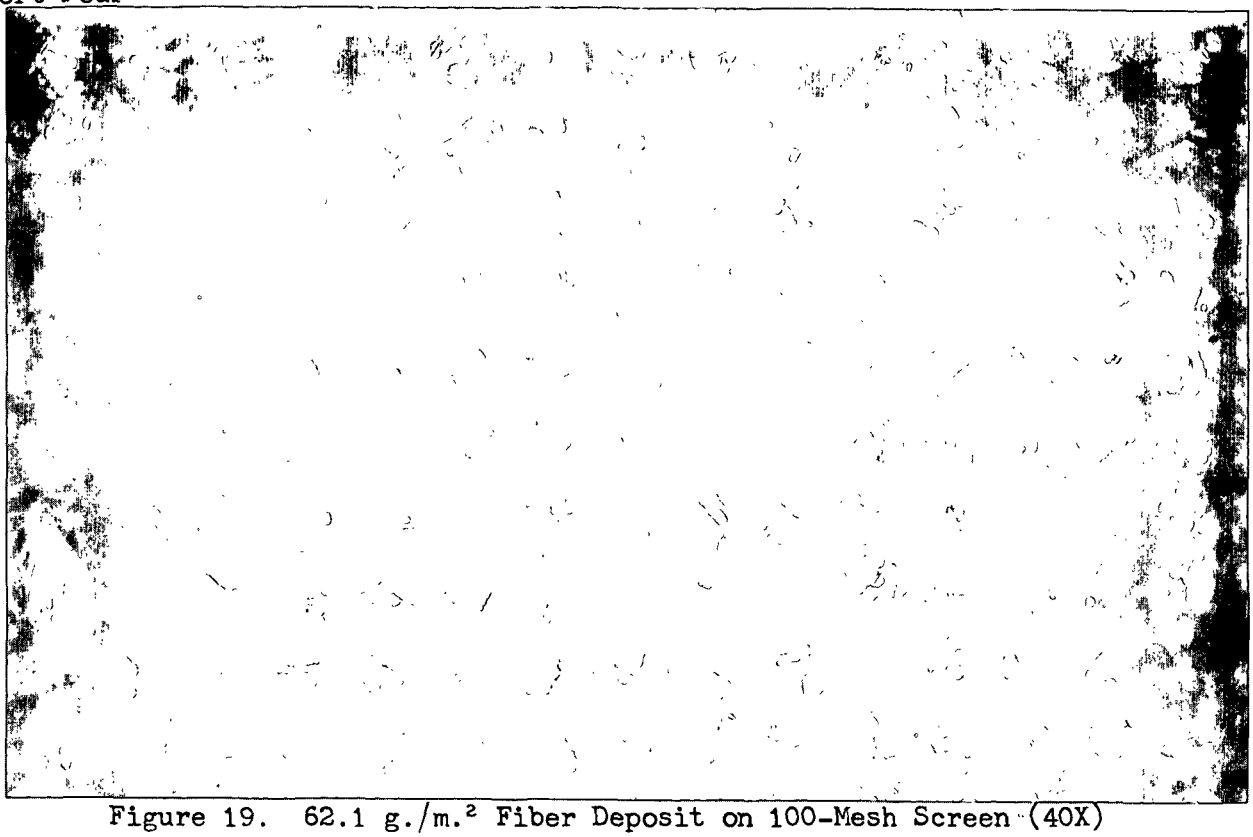

Figure 19. 62.1 g./m.^{2} Fiber Deposit on 100-Mesh Screen (40X)

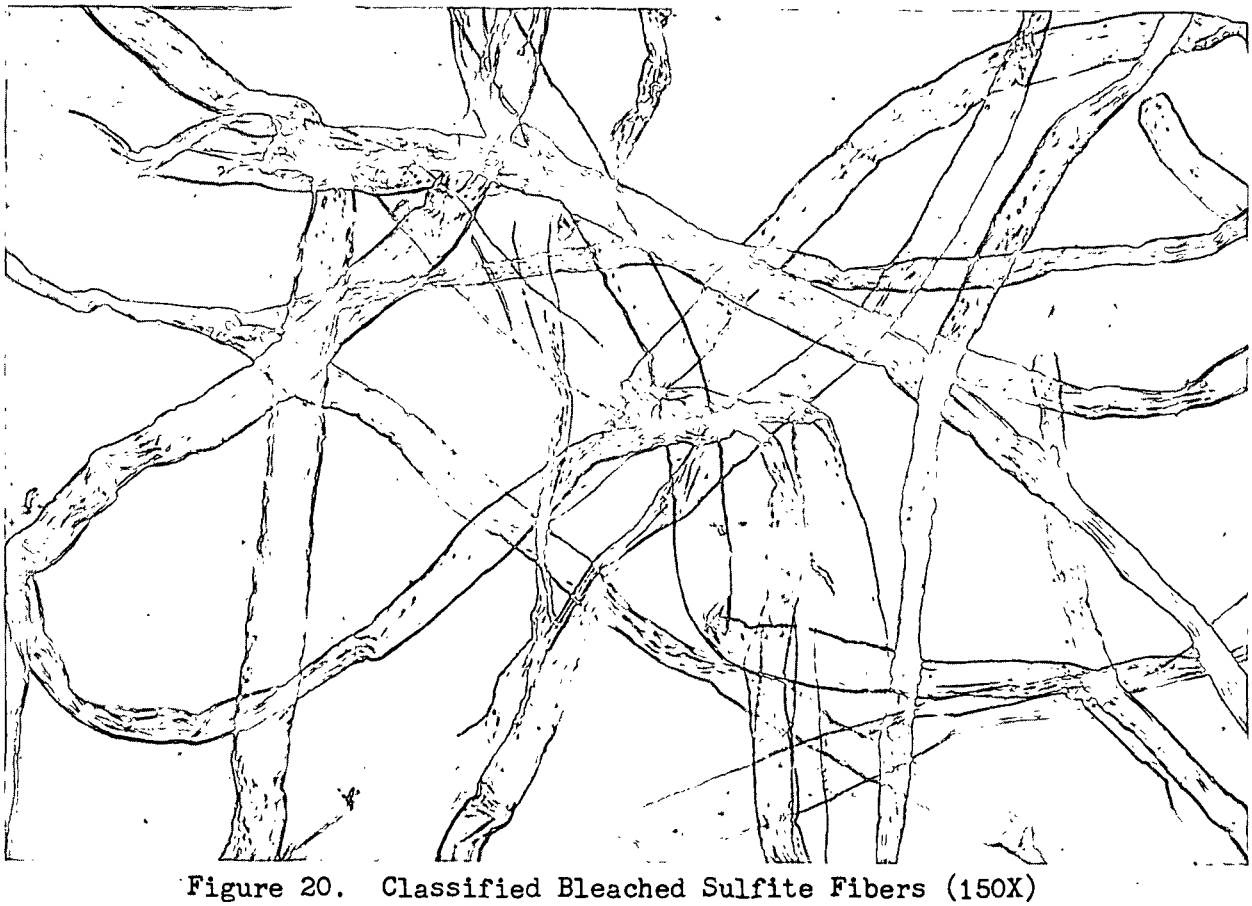

Figure 20. Classified Bleached Sulfite Fibers (150X)

weight. Even at the higher basis weights of 38 and 62 g./m.^{2} in the photomicrographs of Fig. 18 and 19, the equivalent mat thicknesses are probably not greater than about 8-12 fiber diameters. It might be expected that the porosity distribution effect could extend into this basis weight range.

If the assumption is made that this change in porosity distribution in thin mats is alone responsible for the discrepancies between experimental and predicted results for thin mats, a value of an integrating factor, $\underline{I}$, may be substituted for the thick mat integrating factor, $(1 - \frac{N}{2})^2$ in Equation (5) so that

$$\bar{\epsilon} = 1 - Ivc_p \qquad (13).$$

This integrating factor (or porosity distribution factor) is considered to be a function of mat basis weight. It may be calculated by trial and error from experimental data such that the use of this empirical factor in the flow correlation [Equation (8)] will represent one data point in each basis weight curve in Fig. 16. Values were calculated for the empirical integrating factor $\underline{I}$ at a pressure drop of 10^5 dynes/cm.^{2} for each basis weight in Fig. 16. These values of the porosity distribution factor are shown in Fig. 21 as a function of the basis weight together with the two theoretical limits of the porosity distribution factor. As the basis weight approaches zero, the mat must approach a uniform porosity and the integrating factor would equal unity. This is the equivalent of saying that the average porosity flow correlation and the differential form of the flow correlation must become identical as the mat basis weight approaches that corresponding to a differential layer of the order of magnitude of one fiber thickness. The other theoretical limit for porosity distribution factor, $\underline{I}$, for very thick mats would be given by $(1 - \frac{N}{2})^2$ where the value of the compressibility

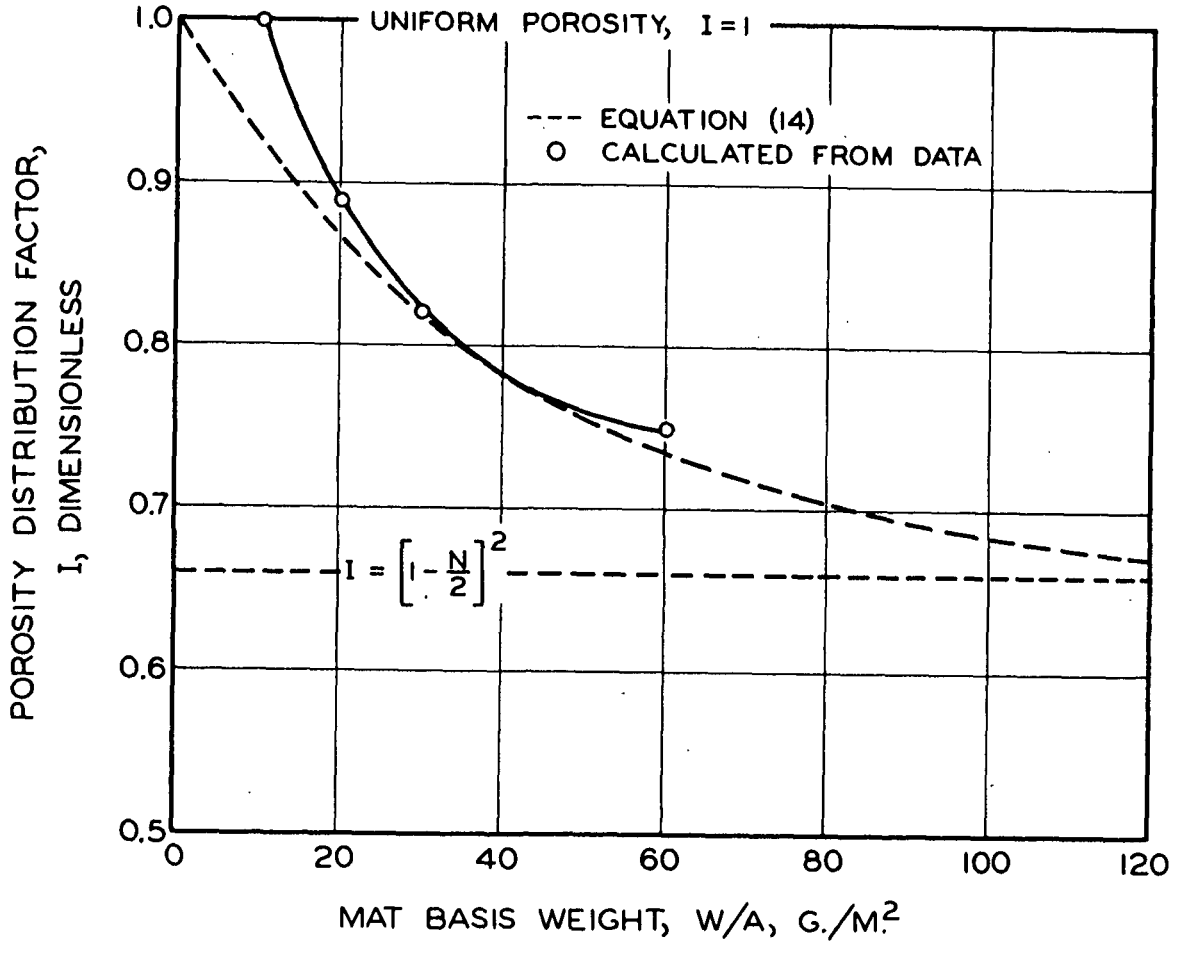

Figure 21. Porosity Distribution Factor

constant $\underline{N}$ is that determined in the mechanical compacting pressure measurements of thick mats. A smooth curve agrees with the data in Fig. 21 in conformity with these two theoretical limits.

This physical picture of the porosity distribution function would be represented by an exponential die-away function of the type $\underline{I} = \underline{m}_1 + \underline{m}_2 \, e^{-\underline{m}_3(\underline{W}/\underline{A})}$. The constants $\underline{m}_1$ and $\underline{m}_2$ should be given by the two limiting cases of porosity distribution when basis weight approaches zero and for thick mats. The third constant, $\underline{m}_3$, must be determined from experimental data. Taking the datum point at a basis weight of 30 g./m.^{2} from Fig. 21 gives

$$I = (1 - \frac{N}{2})^2 + (N - \frac{N^2}{4}) \, e^{-252(W/A)} \qquad (14).$$

This equation for porosity distribution factor is shown in Fig. 21 to agree reasonably well with the data.

Next, using the four data points from Fig. 21 for porosity distribution factor $\underline{I}$, pressure drop-velocity curves have been predicted from Equations (8) and (13) and are shown as dotted lines in Fig. 16. These relationships, modified to account for empirically determined porosity distributions, are seen to agree almost exactly with all the pressure drop-velocity data for thin mats.

This good agreement with the experimental data is encouraging from an empirical standpoint in that it offers a relatively simple possibility for modifying the average porosity flow correlation to account for "fiber-wire interaction." The physical picture upon which it is based is relatively simple in that the porosity distribution factor $\underline{I}$ merely accounts for a gradual change from a uniform porosity in a thin mat to a predictable porosity distribution in a thick mat where the interaction between fiber layers and between fibers and forming wire can be neglected.

This physical picture may be somewhat misleading, however, since it is still possible and even probable that at least two other effects are present in thin mats: (1) flow convergence because of the presence of a forming wire beneath the mat, and (2) change in mat compressibility constants M and N at low mat basis weights. These two effects can be present together with the porosity distribution effect and all three fiber-wire interaction phenomena included together in the empirically determined porosity factor I. Study of the photomicrographs in Fig. 17-19 indicates qualitatively that all three effects could probably be present in thin mats. Even at a basis weight of about 60 g./m.^{2} in Fig. 19, the wires in the forming screen are probably affecting the convergence of flow lines through the mat to give an additional pressure drop over that predicted for thick mats. In compression of thin mats, it seems likely that the absence of enough fibers to bend and deform into open voids would alter the compressibility constants M and N over that measured for thick mats. If, in fact, compressibility constants M and N were available for thin mats, the empirical porosity distribution curve I in Fig. 16 would be altered. One of the most pressing needs in future work is to obtain data for thin mat compression behavior, i.e., mats below about 100 g./m.^{2} Only then can the exact physical picture of fiber-wire interaction be further clarified.

Recently Manson and Mardon (12) and Wahlstrom and O'Blenes (13) have developed drainage testers to conduct high-velocity, constant-pressure filtrations in "practical papermaking" consistency ranges. The results of tests with wood pulps have been treated by empirical curve fitting. Although the testers are ingeniously constructed to perform short-time filtrations, the simultaneous interaction of many unknown variables such as flocculation, incomplete retention, fines distribution, variable velocity, and fiber-wire interaction make interpretation of

the data confusing. In fact, the authors have arrived at completely opposite conclusions, each of which is in conflict with the results of this study. The reasons for the apparent discrepancies can be demonstrated in the following manner.

By utilizing the fact that any relationship between two variables (no matter how complex) can be made to approximate a linear relationship by reducing the range of the variables, a relatively "easy-to-use" equation can be developed to force fit the drainage data and relate fluid pressure drop, fluid velocity, and mat basis weight. For example, in the logarithmic representation of data in Fig. 16, the pressure drop and velocity data are obviously concave upward, but over a pressure drop range from about 10^{4} to 10^{5} dynes/cm.^{2}, the data can be approximated by parallel straight lines. Similarly, representing the original constant-rate filtration data from Fig. 14 on logarithmic scales shows in Fig. 22 that over a basis weight range of about 10 to 70 g./m.^{2} parallel lines will approximate the concave upward form of the data. As shown in Appendix VII, this leads to the empirical relationship

$$\Delta P = k' U^{n} (W/A)^{m} \qquad (15),$$

where average values of the empirical constants are determined to be

$\underline{k}' = 1.68 \times 10^{4}$,

$\underline{n} = 2.60$, and

$\underline{m} = 1.46$.

Comparing this empirical representation of the data to the modified hydraulic radius flow correlation, e.g., Equations (8) and (13), show that the exponent of basis weight of 1.46 (larger than unity) has absorbed the effect of fiber-wire interaction. On the other hand, the exponent of 2.60 of velocity has absorbed the effects of mat compressibility and the relative amounts of viscous and inertial flow, and partially absorbed the fiber-wire interaction effect of

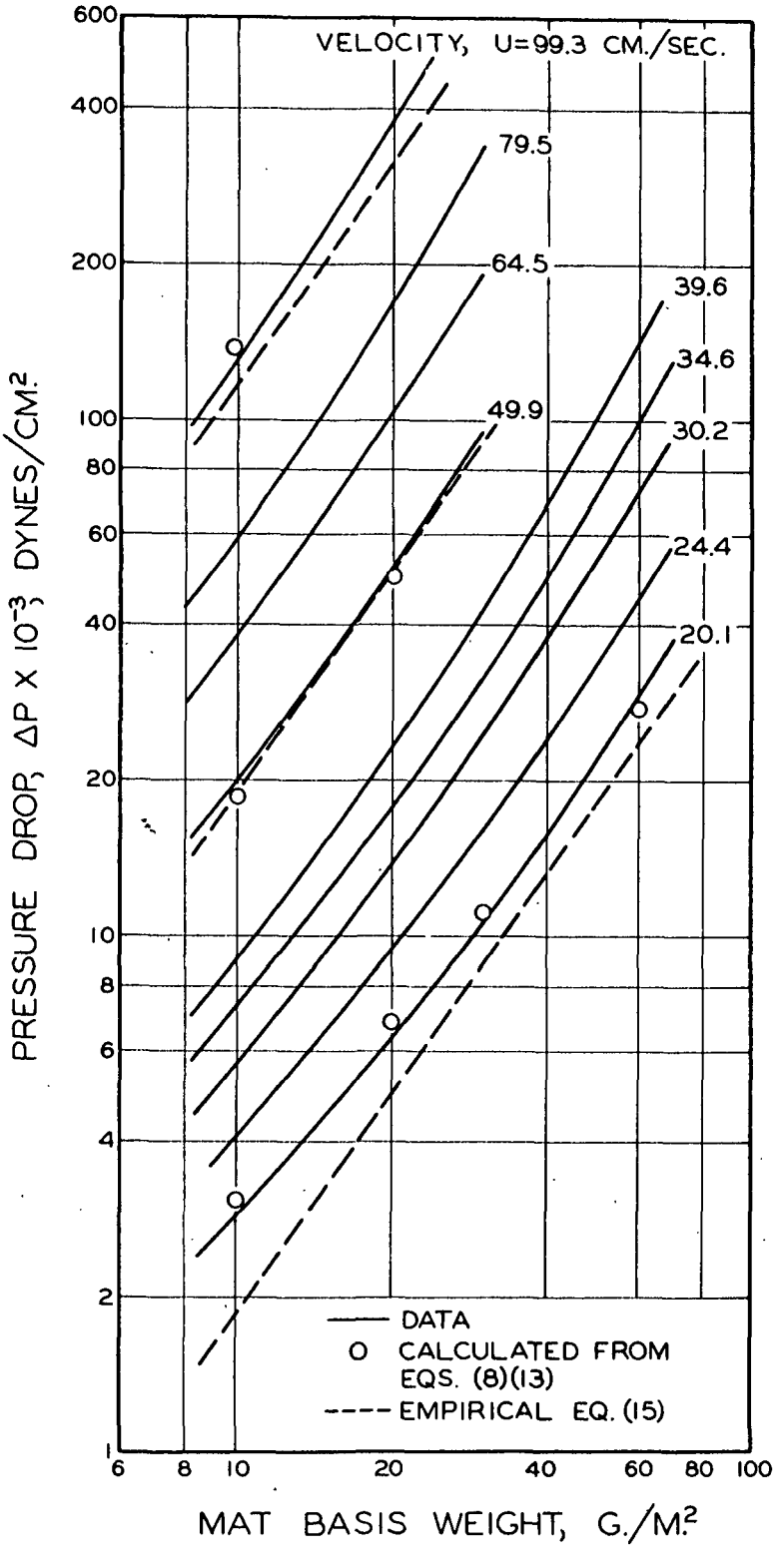

Figure 22. Pressure Drop as a Function of Basis Weight

changing porosity distribution. Mardon (12) has simplified Meadley's (14) previous orifice model correlation to represent wood pulp data by

$$\Delta P = \left(\frac{\mu}{K}\right) U^{\psi} \qquad (16),$$

where μ/K is called a drainage coefficient. Mardon states:

> "The exponent ψ is related to the nature of the flow through the fibre bed and theoretically must lie between 1 and 2. For the case of ψ equals 1 the flow is laminar and for ψ equals 2 the flow is turbulent. In most cases the average flow is neither truly laminar nor turbulent but somewhere between. Therefore the value of ψ usually lies between 1 and 2. It should be pointed out that for highly compressible mats the value of ψ can exceed 2."

It was previously noted by the authors of this report that ψ depends upon basis weight and the pressure range (4). In addition, ψ can be greater than 2 for only slightly compressible mats of synthetic fibers (24). Also ψ can vary between 1 and greater than 2 for a variety of flow regimes representing everything between purely viscous flow with negligible inertial effects and transition flow where inertial effects predominate. It is doubtful that true turbulent flow is ever reached in fiber mats. Manson and Mardon (12) have reported ψ values from 0.7 to 1.8 for various wood pulps under various test conditions compared to a velocity exponent from Equation (15) of 2.6 over the stated pressure and basis weight range for the classified bleached sulfite pulp of this study.

In Fig. 23, the relative pressure drops over the forming wire and over the mat because of viscous and inertial effects are shown for a constant-rate mat formation at 40 cm./sec. using data from Fig. 16 and Equations (8) and (13). The pressure drop over the wire is significant during the whole formation period but falls off rapidly as the basis weight increases, until at 60 g./m.^{2} it is about 10% of the total. The pressure drop over the mat because of viscous resistance

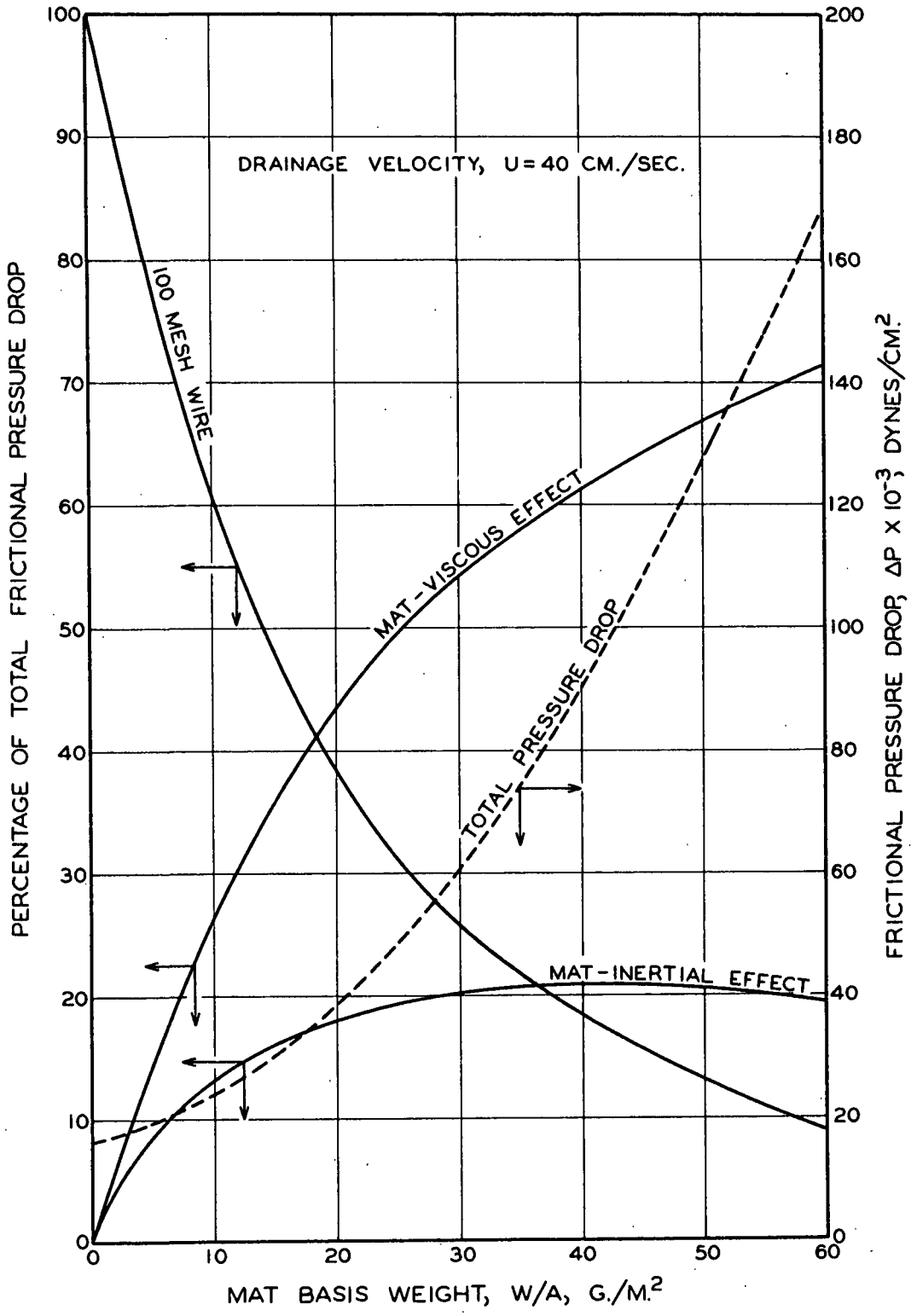

Figure 23. Frictional Pressure Drop Distribution

increases throughout the formation, and amounts to about 70% of the total at the final basis weight. The inertial resistance of the mat increases rapidly to about 20% of the total during the initial formation stages and then remains essentially constant from a basis weight of about 20 to 60 g./m.^{2} Even at this relatively high flow velocity of 40 cm./sec., the inertial resistance never amounts to more than 33% of the total mat resistance. Even at a velocity of 90 cm./sec., the inertial effect only increases to a maximum value of 36% of the total mat resistance because of the additional mat compression (as can be calculated from the data of Fig. 16).

The other workers, Wahlstrom and O'Blenes (13), correlated their data during the approximately constant-pressure period of mat formation from about 30 to 70 g./m.^{2} with the empirical equation for forming time, t, given by

$$t = \frac{G}{s} \Delta P^{-\beta} (W/A)^{\alpha} \qquad (17),$$

where G is a drainage coefficient and s is the slurry consistency. As shown in Appendix VII, this form of the constant pressure filtration equation may be derived by integration of the empirical flow equation (15) to give

$$t = \frac{(k')^{1/n}}{(1 + m/n)\rho s} \Delta P^{-1/n} (W/A)^{1+m/n} \qquad (18),$$

where by comparing to Equation (17) it is seen that

$$G = \frac{(k')^{1/n}}{(1 + m/n)\rho}, \quad \alpha = 1 + m/n, \text{ and } \beta = 1/n.$$

Wahlstrom and O'Blenes reported values of β from 0.35 to 0.53, and values of α from 1.7 to 3.5, for various wood pulps over a pressure range of from 0.5 to 6 x 10^5 dynes/cm.^{2} The corresponding values of β and α from this study of

classified bleached sulfite pulp are 0.38 and 1.56, respectively. Wahlstrom and O'Blenes said that α described the effect of pressure and compression, whereas β described the rate of mat formation, depending mainly on pulp type and degree of beating. Furthermore, they mistakenly concluded that the flow was laminar and that values of β^{α} greater than 2 were caused by fines migration, and values less than 2 were caused by velocity gradient in the mat. Although these latter two effects may be present, Wahlstrom and O'Blenes' conclusions about their effect on drainage are seriously in error because of the interaction of fiber and wire effects, among other things. The study of fines retention must be carried out under carefully controlled and understood hydrodynamic conditions, as presented in Report Three of this project (15). Also the important differences in mechanisms of fiber and fines retention must be recognized. Velocity gradient effects can be predicted by solution of the equation of continuity and the modified hydraulic radius flow correlation. This has been done for purely viscous flow at low velocity and confirmed experimentally (16), and is presently being carried out under this project for transition flow.

While empirical curve fitting has the obvious advantage of often giving a deceptively simple equation representing experimental data over the range of the data, general conclusions about internal mechanisms from such results can never be proved and, as illustrated above, are often conflicting and misleading. The simple advantage of the empirically developed Equation (15) is illustrated in Fig. 22 where it can be seen to agree with three arbitrarily chosen constant-rate filtrations within about $\pm$15%. The modified hydraulic radius flow correlation in Equation (8) fits the data much better, as seen in Fig. 16 and 22, and has the more important advantage of isolating the effects of fiber properties, mat properties, fluid properties, and flow conditions. The present understanding and quantitative

representation of fiber-wire interaction needs further clarification and isolation of relative contributions of porosity distribution, flow convergence, and thin mat compression effects.

FUTURE WORK

To further clarify fiber-wire interaction phenomena in the formation of thin wood pulp fiber mats, it will be necessary to obtain data for the compression behavior of low basis weight (less than 100 g./m.^{2}) fiber mats. Work has been under way on this phase of the project, but accurate and reproducible results have not been attained as yet. Modifications in the compression apparatus are currently being made, and studies on compression behavior of thin mats will be continued in the future. Once these data are available, the possible effect of changing compressibility constants with decreasing basis weight can be isolated in the empirical porosity distribution factor proposed in this study.

Then, by studying wires of various diameters and structures, it will be possible to ascertain the influence of forming wire on flow convergence and obtain numerical values for the porosity distribution factor. By studying a number of carefully selected wood pulps and several types of forming wires, it should be possible to obtain the necessary data to develop a quantitative relationship for the porosity distribution factor which would combine the effects of varying porosity distribution in thin mats and the effects of different wires on flow convergence.

Currently, work is under way to obtain more hydrodynamic data from the dynamic drainage tester and to measure thin mat compression response. A possible alternate approach in the treatment of the experimental data is being pursued in which the wire and thin fiber mat deposit are treated as a single, interacting system using direct experimental data of the measured pressure drop over both the wire and fiber deposit in the data analysis. In the method of interpretation used in this and previous reports, the pressure drop measured separately over the bare forming wire has been subtracted from the experimentally measured over-all pressure drop to obtain the total compacting pressure which acts across the fiber mat.

There are, of course, some theoretical objections to this procedure since the relative size of fibers and the individual wires used to weave the forming screens are such that the initial fiber deposits at very low basis weights actually penetrate into the weave of the forming screens and give rise to the so-called fiber-wire interacting system.

Because in the previous study of synthetic fibers and in this study of wood pulp fibers no significant effect of pore size distribution on mat permeability has been found, and because both the past theoretical review (5) and recent experimental data by Bliesner (8) have indicated not much effect of pore-size distribution on permeability, the previously proposed objective of determining the pore-size distribution in thin mats will not be attempted. Work in the academic program is still under way on direct observation of fiber movement in thick mat compression, and attempts under this project to initiate studies of individual wood pulp fibers under compression in thick mats will not be attempted at this time.

In the immediate future it is hoped that studies under the academic research program can be initiated to investigate (1) the effect of fiber shape on flow resistance and contact area, (2) the effect of mat compression on fiber contact area, (3) the effect of mat compression on fiber deswelling at points of contact, and (4) further attempts to prepare fully water-swollen wood pulp fiber cross sections for direct microscopic observation and measurement. Satisfactory completion of these latter studies will increase understanding of fiber mat behavior during sheet forming, but at this time are beyond the scope of the sheet-forming project.

NOMENCLATURE

A = area perpendicular to flow, cm.^{2}

A_n = nth coefficient in Gaussian quadrature formula

a = a constant, c.g.s. units

b = a constant, c.g.s. units

c_p = mat density, g./cc.

F, f = functions

G = drainage coefficient, c.g.s. units

I = porosity distribution factor, dimensionless

K = drainage factor, c.g.s. units

k = Kozeny factor, dimensionless

k' = a constant, c.g.s. units

M = compressibility coefficient, c.g.s. units

m = mass wet mat per mass dry mat, g./g.; a constant

N = compressibility constant, dimensionless

n = a constant

ΔP, Δp = frictional pressure drop, dynes/cm.^{2}

S_v = specific surface, volume basis, cm.^{2}/cc.

S_w = specific surface, mass basis, cm.^{2}/g.

s = slurry consistency, g./g.

s' = filtrate consistency, g./g.

t = time, sec.

t_n = nth Gaussian fraction of integration range

U = superficial velocity, cm./sec.

V = filtrate volume, cc.; a factor of pressure drop

v = swollen fiber specific volume, cc./g.

$\underline{W}$, $\underline{w}$ = mass of fibers, g.

$\underline{Y}_{\underline{n}}$ = nth value of integrant for Gaussian spacing

α = a constant, dimensionless

β = a constant, dimensionless

ϵ = mat porosity, dimensionless

μ = viscosity, poises

ρ = density, g./cc.

τ = a factor of time, sec.

ϕ = function

ψ = a constant, dimensionless

ACKNOWLEDGMENT

The authors wish to acknowledge the assistance of L. White, O. Kuehl, and J. Hankey in carrying out experimental work and the assistance of H. Meyer in the mathematical analysis.

LITERATURE CITED

1. Project 2348, Progress Report One, Studies of the sheet-forming process--Dynamic drainage, March 1, 1963.

2. Project 2348, Progress Report Two, Studies of the sheet-forming process--Permeation of thin fiber mats, March 29, 1963.

3. Graff, J. H., Paper Trade J. 117, no. 17:25(Oct. 21, 1943).

4. Ingmanson, W. L., and Andrews, B. D., Tappi 46, no. 3:150(1963).

5. Project 2348, Permeation, Draft chapter, 1962.

6. Project 2348, Filtration, Draft chapter, 1963.

7. Ingmanson, W. L., Andrews, B. D., and Johnson, R. C., Tappi 42, no. 10:840 (1959).

8. Bliesner, W. C. A study of the porous structure of fibrous sheets using permeability techniques. Doctoral Dissertation. Appleton, Wis., The Institute of Paper Chemistry, 1963.

9. Onogi, S., and Sasaguri, K., Tappi 44, no. 12:874(1961).

10. Van den Akker, J. A. In Bolam's The formation and structure of paper. Vol. I. p. 205. London, England, Tech. Sect. British Paper and Board Makers' Association, 1962.

11. Project 2348, Compression, Draft chapter, 1963.

12. Manson, D. W., and Mardon, J., Pulp Paper Mag. Can. 63, no. 5:259(1962).

13. Wahlstrom, B., and O'Blenes, G., Pulp Paper Mag. Can. 63, no. 8:405(1962).

14. Meadley, C. K., Can. J. Chem. Eng. 40, no. 6:256(1962).

15. Project 2348, Progress Report Three, Studies of the sheet-forming process--The retention of fine particles in fiber mats, Jan. 20, 1964.

16. Project 2210, Progress Report Fifteen, The dynamic behavior of pulps--The drainage of fiber networks: The effect of slurry consistency on mat structure, Oct. 25, 1963.

THE INSTITUTE OF PAPER CHEMISTRY
Engineering and Technology Section

William L. Ingmanson

William L. Ingmanson

Bruce D. Andrews

Bruce D. Andrews

APPENDIX I

MICROSCOPIC DATA AND AVERAGE FIBER MASS RESULTS

TABLE I-I

FIBER PERIMETERS

Number of Fibers	Perimeter, microns
1	44
2	48
2	52
1	55
7	60
3	64
5	67
5	69
1	72
5	75
2	78
12	80
5	84
7	87
4	90
6	93
6	97
8	100
6	103
5	107
5	110
3	113
6	120
5	127
6	133
1	140
3	147
1	153
1	156
1	160
1	180
Total: 121	Arith. Av.: 95

TABLE I-II

FIBER LENGTH DISTRIBUTION

Interval, mm.	Frequency	(a) Frequency, %	(b) Average Length, mm.	a · b
0.1-0.2	1	0.1	0.15	0.02
0.2-0.4	12	0.9	0.3	0.27
0.4-0.6	35	2.7	0.5	1.35
0.6-0.8	53	4.0	0.7	2.80
0.8-1.0	71	5.4	0.9	4.86
1.0-1.2	82	6.2	1.1	6.82
1.2-1.4	129	9.8	1.3	12.74
1.4-1.6	138	10.5	1.5	15.75
1.6-1.8	86	6.5	1.7	11.05
1.8-2.0	89	6.8	1.9	12.92
2.0-2.2	95	7.2	2.1	15.12
2.2-2.4	81	6.2	2.3	14.26
2.4-2.6	82	6.2	2.5	15.50
2.6-2.8	82	6.2	2.7	16.74
2.8-3.0	57	4.3	2.9	12.47
3.0-3.2	40	3.0	3.1	9.30
3.2-3.4	36	2.7	3.3	8.91
3.4-3.6	53	4.0	3.5	14.00
3.6-3.8	31	2.4	3.7	8.88
3.8-4.0	28	2.1	3.9	8.19
4.0-4.2	16	1.2	4.1	4.92
4.2-4.4	9	0.7	4.3	3.01
4.4-4.6	3	0.2	4.5	0.90
4.6-4.8	6	0.5	4.7	2.35
4.8-5.0	1	0.1	4.9	0.49
5.0-5.2	1	0.1	5.1	0.51
	1317			204.13

Arithmetic average fiber length = Σ ab/100 = 2.04 mm.

TABLE I-III

FIBER MASS BY DILUTION TECHNIQUE

Sample	No. of Fibers	Final Concentration, g./g. slurry	Total Mass of Slurry, g.	Fiber Mass, g./fiber
1	430	1.472×10^{-6}	102.5	3.51×10^{-7}
2	467	1.472×10^{-6}	114.0	3.59×10^{-7}
3	463	1.521×10^{-6}	115.0	3.78×10^{-7}
4	423	1.521×10^{-6}	99.0	3.57×10^{-7}
			Average:	3.61×10^{-7}

APPENDIX II

RECTIFIED CONSTANT-RATE FILTRATION EQUATION FOR VISCOUS FLOW

The previously developed (5) permeation equation for viscous flow of an isothermal, incompressible fluid through a compressible fiber mat is

$$\frac{\Delta P}{W/A} = \frac{\bar{k}(1 - \bar{\epsilon})vS_v^2}{\bar{\epsilon}^3}\mu U \qquad \text{(II-1)}$$

where

ΔP = pressure drop over the mat,

W/A = basis weight of mat,

v = fiber specific volume,

S_v = fiber specific surface (volume basis),

U = superficial fluid velocity,

μ = fluid viscosity,

$\bar{\epsilon} = 1 - (1 - \frac{N}{2})^2 vc_p$, average mat porosity (II-2)

$\bar{k} = 3.5 \frac{\bar{\epsilon}^3}{(1 - \bar{\epsilon})^{1/2}} [1 + 57(1 - \bar{\epsilon})^3]$, average Kozeny factor, (II-3)

c_p = mat solids concentration at compacting pressure equivalent to ΔP,

$c_p = M(\Delta P)^N$, and (II-4)

M, N = mat compressibility constants.

This relation is applied to a filtration by expressing the basis weight of the mat being formed as a function of filtration time through a material balance (6),

$$\frac{W}{A} = \frac{\rho(s - s')}{1 - ms} Ut \qquad \text{(II-5)},$$

where

$\underline{s}$ = slurry consistency,

$\underline{s}'$ = white water consistency,

$\underline{m}$ = average mat moisture content, mass wet mat per mass dry mat,

$\underline{t}$ = filtration time, and

ρ = fluid density.

In the constant-rate filtration of a dilute slurry ($\underline{s} < 0.1\%$) with complete fiber retention ($\underline{s}' = 0$), the fluid velocity is constant, and Equation (II-5) may be simplified to

$$\frac{W}{A} \simeq \rho s U t \qquad \text{(II-6)}.$$

Combining Equations (II-1, -2, -3, and -6) and rearranging gives

$$\frac{\Delta P}{c_p^{1/2} t} = 3.5(1 - \frac{N}{2})v^{3/2} S_v^2 \mu \rho s U^2 \left\{1 + 57[(1 - \frac{N}{2})^2 v]^3 c_p^3\right\} \qquad \text{(II-7)}.$$

This is a linear relationship of the form

$$\frac{\Delta P}{c_p^{1/2} t} = m_1 + m_1 m_2 c_p^3 \qquad \text{(II-8)}$$

when the left-hand member is shown as a function of $\underline{c_p^3}$ and $\underline{m_1}$ and $\underline{m_2}$ are constants given by

$$m_1 = 3.51(1 - \frac{N}{2})v^{3/2} S_v^2 \mu \rho s U^2, \text{ and} \qquad \text{(II-9)}$$

$$m_2 = 57[(1 - \frac{N}{2})^2 v]^3 \qquad \text{(II-10)}.$$

The $\underline{c_p^3} = 0$ intercept is $\underline{m_1}$ and the slope of the straight line is $\underline{m_1 m_2}$. Thus, simple intercept and slope measurements of data correlated with Equation (II-8) may

be used to calculate specific surface, $\underline{S}_{\underline{v}}$, and specific volume, $\underline{v}$, by solving Equations (II-9) and (II-10).

$$v = \left(\frac{m_2}{57}\right)^{1/3} \frac{1}{\left(1 - \frac{N}{2}\right)^2} \qquad \text{(II-10)}$$

$$S_v = \left(\frac{m_1}{\mu \rho s U^2 3.5 \left(1 - \frac{N}{2}\right) v^{3/2}}\right)^{1/2} \qquad \text{(II-9)}.$$

Specific surface may be expressed on a volume $(\underline{S}_{\underline{v}})$ or a mass basis $(\underline{S}_{\underline{w}})$. The interrelationship is given by

$$S_w = v S_v \qquad \text{(II-11)}.$$

APPENDIX III

AVERAGE POROSITY DEVELOPMENT FROM VISCOUS FLOW CORRELATION

The modified hydraulic radius theory leads to the following differential flow equation (5) for viscous flow:

$$\frac{d(\Delta p)}{d(w/A)} = \frac{k(1-\epsilon)vS_v^2}{\epsilon^3}\mu U \qquad \text{(III-1)}.$$

We wish to define an average porosity so that

$$\frac{\Delta P}{W/A} = \frac{\bar{k}(1-\bar{\epsilon})vS_v^2}{\bar{\epsilon}^3}\mu U \qquad \text{(II-1)}.$$

Since in filtrations of dilute slurries ($\underline{s} < 0.1\%$) the superficial velocity, $\underline{U}$, is constant throughout the mat (16), Equations (III-1) and (II-1) may be related so that

$$\int_0^{\Delta P} \frac{d(\Delta p)}{k(1-\epsilon)/\epsilon^3} = \frac{\Delta P}{\bar{k}(1-\bar{\epsilon})/\bar{\epsilon}^3} = \phi(\epsilon) \qquad \text{(III-2)}.$$

Substituting the porosity dependency equation for Kozeny factor (7) of

$$k = 3.5\frac{\epsilon^3}{(1-\epsilon)^{1/2}}[1 + 57(1-\epsilon)^3] \qquad \text{(III-3)}$$

into the left-hand side of Equation (III-2) gives

$$\int_0^{\Delta P} \frac{d(\Delta p)}{3.5(1-\epsilon)^{1/2}[1 + 57(1-\epsilon)^3} = \phi(\epsilon) \qquad \text{(III-4)}.$$

This integral can be found analytically for only two special cases: (1) when porosity is greater than 0.9 and the term in brackets in Equation (III-4) is

approximately equal to unity or (2) when the Kozeny factor, as in Equation (III-2) is constant.

For Case (1), Equation (III-4) becomes

$$\phi(\epsilon) \cong \int_0^{\Delta P} \frac{d(\Delta p)}{3.5(1 - \epsilon)^{1/2}} \quad \text{for} \quad \epsilon > 0.9 \qquad \text{(III-5)}.$$

Substituting for solid fraction from

$$(1 - \epsilon) = vM(\Delta p)^N \qquad \text{(III-6)}$$

and integrating Equation (III-5) gives, when compared to Equation (III-2),

$$(1 - \bar{\epsilon}) \cong (1 - \frac{N}{2})^2 vM\Delta P^N \quad \text{for} \quad \epsilon > 0.9 \qquad \text{(III-7)}.$$

For Case (2), integration of the left side of Equation (III-2) gives

$$\frac{1 - 3v(1 - N)c_p + 3v^2 \frac{(1 - N)}{(1 + N)} c_p^2 - v^3(\frac{1 - N}{1 + 2N})c_p^3}{(1 - N)vc_p} = \frac{\bar{\epsilon}^3}{(1 - \bar{\epsilon})} \qquad \text{(III-8)}.$$

The numerator of the left side of Equation (III-8) can be approximated by a simpler cubic equation so that

$$\frac{[1 - (1 - N)vM\Delta P^N]^3}{(1 - N)vM\Delta P^N} \cong \frac{\bar{\epsilon}^3}{(1 - \bar{\epsilon})} \qquad \text{(III-9)},$$

and therefore,

$$1 - \bar{\epsilon} = (1 - N)vM\Delta P^N \quad \text{when} \quad \underline{k} = \text{constant} \qquad \text{(III-10)}.$$

Since Equation (III-3) shows that $\underline{k}$ is nearly constant for porosities from 0.6 to about 0.8 and since

$$(1 - \frac{N}{2})^2 \cong (1 - N) ,$$

the average porosity for use in Equation (III-1) is defined by

$$\bar{\epsilon} = 1 - (1 - \frac{N}{2})^2 M \Delta P^N \qquad \text{(III-11)} .$$

The accuracy of this average porosity definition can be checked by numerical integration and comparison of porosity functions, $\phi(\epsilon)$ in Equation (III-2).

APPENDIX IV

DIGITAL COMPUTER SOLUTION OF FLOW EQUATION [a]

The modified hydraulic radius theory and Reynolds concept of considering pressure gradient for curved flow equivalent to the sum of viscous and inertial forces leads to the differential flow equation (4, 5),

$$\frac{d(\Delta p)}{d(w/A)} = \frac{k(1-\epsilon)}{\epsilon^3} vS_v^2 \mu U + \frac{b'\sqrt{k}\, vS_v \rho U^2}{\epsilon^3} \qquad \text{(IV-1)}.$$

Separating the variables and writing in integral form gives

$$\int_0^{\Delta P} \frac{\epsilon^3 d(\Delta p)}{\sqrt{k}\left[\sqrt{k}(1-\epsilon)\frac{\mu}{\rho} S_v U + b'U^2\right]} = \rho v S_v (W/A) \qquad \text{(IV-2)}$$

or

$$\int_0^{\Delta P} f(U, \Delta p)\, d(\Delta p) = \rho v S_v (W/A) \qquad \text{(IV-3)}.$$

Kozeny factor, k, and porosity, ϵ, are given by Equations (III-3) and (III-6), respectively. It is desired to calculate the velocity, U, for specified fiber properties as a function of ΔP for different parameters of basis weight, W/A, so that Equation (IV-2) is satisfied. Using Gauss's quadrature formula gives

$$\int_0^{\Delta P} f(U, \Delta p)\, d(\Delta p) = \Delta P(A_1 Y_1 + A_2 Y_2 + \ldots A_n Y_n) \qquad \text{(IV-4)}$$

where

$$Y_n = f(\Delta P \cdot t_n, U) \qquad \text{(IV-5)}$$

---

[a] This work was done by H. Meyer of the Institute faculty, Engineering and Technology Section.

and the $\underline{t}$ and $\underline{A}$ values are given constants obtainable from the literature. For $\underline{n}$ equal to 6,

$\underline{t}_1$	0.0337652	$\underline{A}_1$	0.0856622
$\underline{t}_2$	0.1693953	$\underline{A}_2$	0.1803808
$\underline{t}_3$	0.3806904	$\underline{A}_3$	0.2339570
$\underline{t}_4$	0.6193096	$\underline{A}_4 = \underline{A}_3$	
$\underline{t}_5$	0.8306047	$\underline{A}_5 = \underline{A}_2$	
$\underline{t}_6$	0.9662347	$\underline{A}_6 = \underline{A}_1$	

For a given $\underline{\Delta P}$, we may write Equation (IV-3) as

$$F(U) = \int_0^{\Delta P} f(U,\Delta p)d(\Delta p) - \rho v S_v(W/A) = 0 \qquad \text{(IV-6)}.$$

Thus,

$$F'(U) = \int_0^{\Delta P} \frac{\partial f}{\partial U}\, d(\Delta p) \qquad \text{(IV-7)},$$

and as an improved root, where $\underline{U}_o$ is a first approximation,

$$U_1 = U_o - \frac{F(U_o)}{F'(U_o)} \qquad \text{(IV-8)},$$

and so forth.

The integral in Equation (IV-7) is solved with the same procedure as given in Equation (IV-4). The process, according to Equation (IV-8), is to be repeated until deviations between consecutive roots become smaller than an admissible error.

APPENDIX V

DYNAMIC DRAINAGE TESTER SAMPLE CALCULATIONS

Data are presented for Run A-6 (Table V) made with the dynamic drainage tester with classified bleached sulfite pulp. A sample calculation is given below for one of the data points.

Figure 24 gives the forming wire pressure drop calibration and Fig. 25 shows the pressure drop trace during Run A-6 for the following conditions:

Pressure sensitivity	2 mv./cm. = 40 cm. water/cm. deflection
Chart speed	125 mm./sec.
Total run time	1.981 sec.
Total piston travel	78.52 cm.
Total tube volume	4150 cc.
Forming area	45.6 $cm.^2$
Total fiber mass	0.3808 g.
Temperature	23.5°C. (μ = 0.925 cp.)

Calculations:

Piston velocity (superficial flow velocity), $\underline{U}$ = (78.52/1981) = 39.6 cm./sec.

Slurry consistency, $\underline{s}$ = (0.3808/4150) = 0.917×10^{-4} g./cc.

Pressure drop across wire (Fig. 24) = 14 cm. water

At time, $\underline{t}$ = 0.585 sec., total pressure drop (Fig. 25) = 1 cm. deflection

= 40 cm. water

Pressure drop across mat, $\frac{\Delta P}{\rho g}$ = 40.0 - 14.0 = 26.0 cm. H_2O

ΔP = (26)(980) = 25.5×10^3 dynes/$cm.^2$

Basis weight, (W/A) = $(0.917 \times 10^{-4})(39.6)(0.585)$ = 21.2×10^{-4} g./$cm.^2$

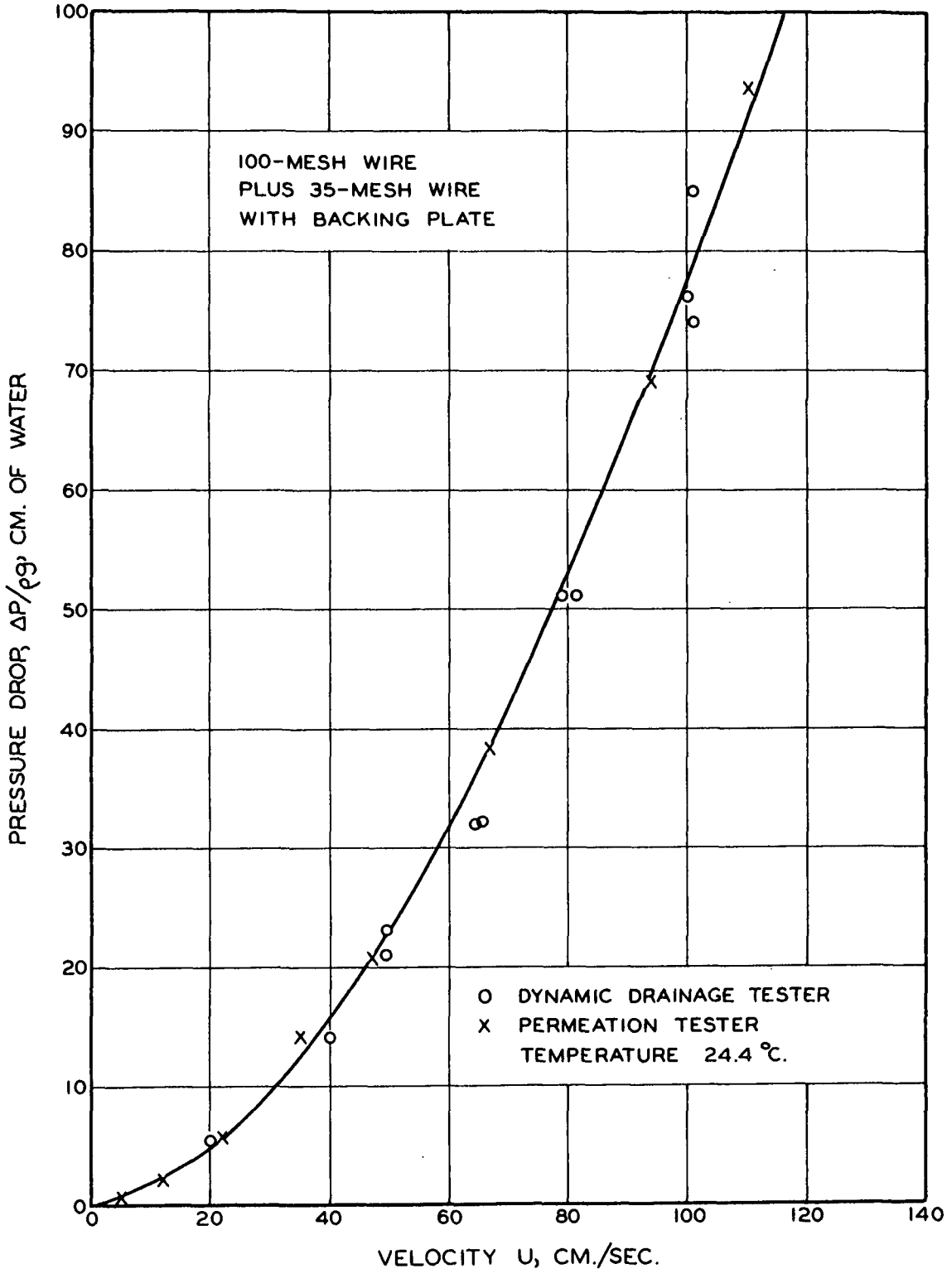

Figure 24. Pressure Drop over Bare Forming Septum Calibration

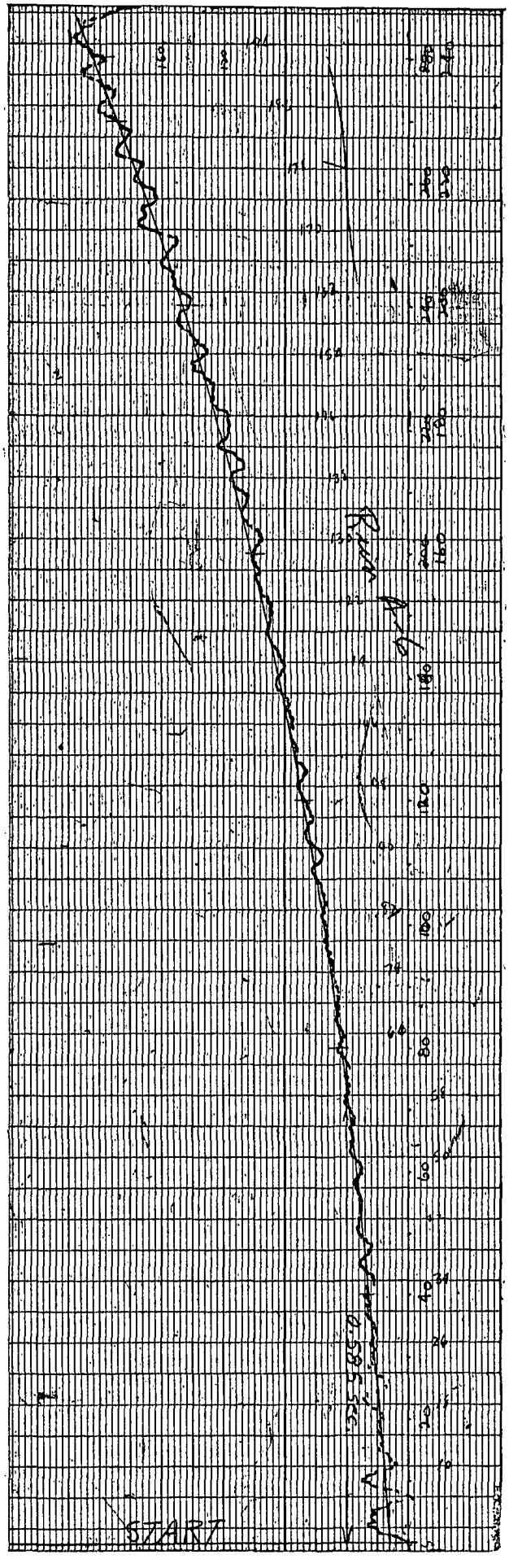

Figure 25. Pressure Drop Trace During Dynamic Drainage Tester Run

APPENDIX VI

ANALOG COMPUTER SOLUTION OF FLOW EQUATION [a]

For determining suitable run conditions in the dynamic drainage tester and for convenience in predicting how certain variables in the flow correlation would affect the constant-rate filtration curve, an analog computer solution of the differential constant-rate filtration flow correlation was developed. The pressure drop *versus* time curves were graphed directly on the *x-y* plotter of the analog computer (Fig. 12 and 13).

Equation (IV-1) is arranged in the following form:

$$\frac{d\Delta P}{dt} = pvS_v U^2 \left\{ \mu S_v \left[\frac{k(1 - \epsilon)}{\epsilon^3} \right] + 0.1 U \rho \frac{k^{1/2}}{\epsilon^3} \right\} \qquad \text{(VI-1)},$$

since for constant-rate filtrations, Equation (II-6) becomes

$$d(W/A) = \rho U s dt \qquad \text{(VI-2)}.$$

Two function generators were used to fit the empirical porosity functions in Equation (IV-1). These were set up as

$$\frac{5k(1 - \epsilon)}{\epsilon^3} \quad \text{and} \quad \frac{5k^{1/2}}{\epsilon^3} \quad \text{vs.} \quad \Delta P$$

using

$$c = c_o + M\Delta P^N, \quad c_o = 0.01$$

for the compressibility relationship. Neither function passes through (0,0) and therefore *y* intercepts must be added; these enter at 7A and 7B in Fig. 26.

---

[a] This work was done by L. White, formerly of the Institute staff, and presently a graduate student at the University of Minnesota.

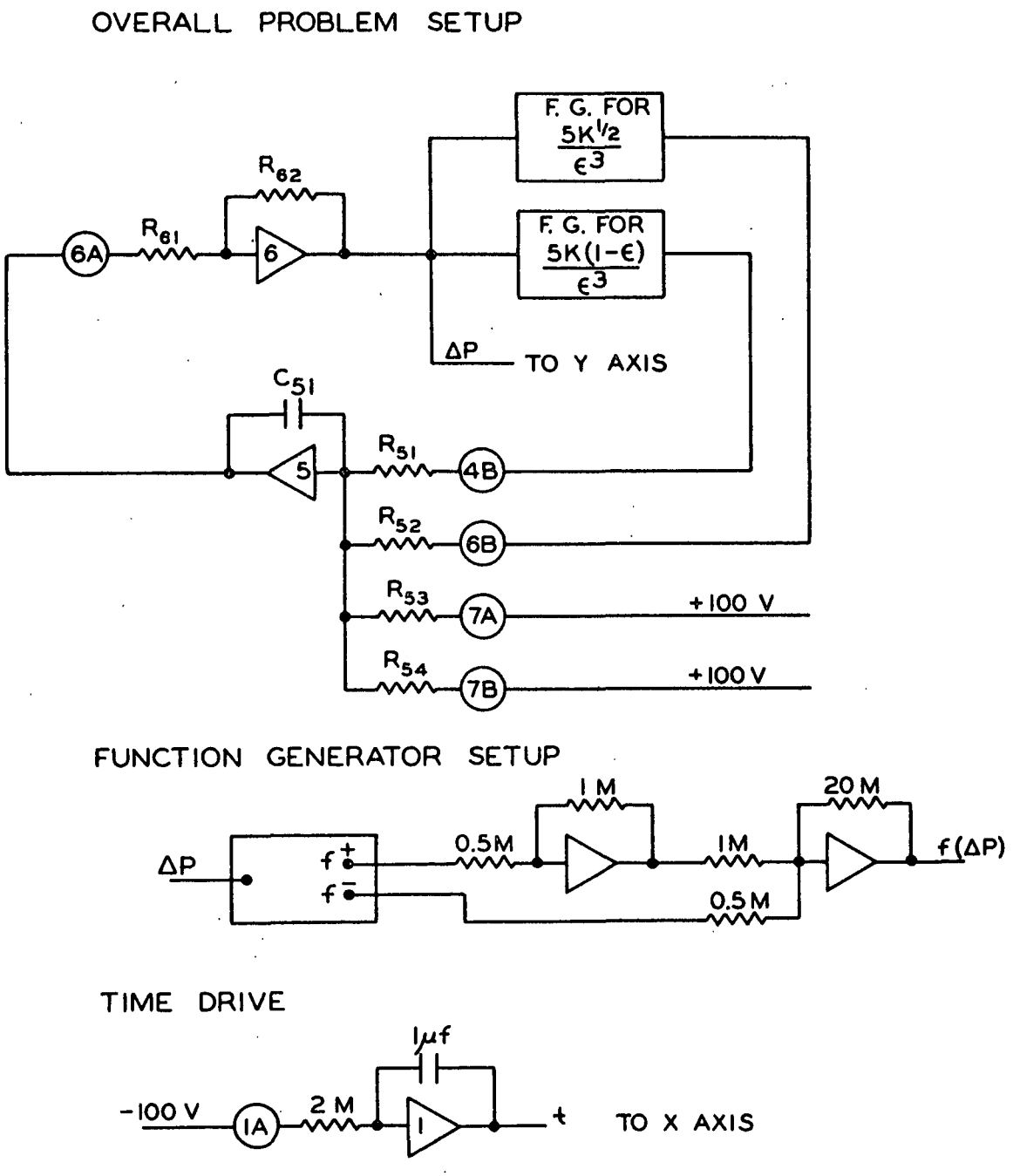

Figure 26. Analog Computer Program

Figures 27 and 28 were used to set the function generators.

The following amplitude and time scale factors were used:

$$100 \text{ volts} = 100{,}000 \text{ dynes/cm.}^2$$

$$\tau = 2t \text{ sec.}$$

(for $20 \leq \underline{U} \leq 40$ cm./sec.). Thus:

$$\frac{dV}{d\tau} = 0.5 \times 10^{-3} \frac{d\Delta P}{dt}$$

$$= 0.5 \times 10^{-2} \rho v S_v U^2 \left\{ \frac{\mu S_v}{50} \left[\frac{5k(1 - \epsilon)}{\epsilon^3} \right] + \frac{0.1U}{50} \left(\frac{5k^{1/2}}{\epsilon^3} \right) \right\} \qquad \text{(VI-3)},$$

where $d\underline{V}/d\tau$ is proportional to $d\Delta\underline{P}/d\underline{t}$. All capacitors were 1μf; values of resistors and potentiometer settings were:

$R_{51} = 1M$

$R_{52} = 10M$

$R_{53} = 20M$

$R_{54} = 20M$

$R_{61} = 1M$

$R_{62} = 5M$

$$6A = 5 \times 10^{-3} v S_v \rho U^2 \frac{R_{61}}{R_{62}}$$

$$4B = \frac{\mu S_v}{50} R_{51} C_{51}$$

$$6B = \frac{U}{500} R_{52} C_{51}$$

$$7A = \frac{5 R_{53} C_{51}}{100} I_1(4B)$$

$$7B = \frac{5 R_{54} C_{51}}{100 R_{52} C_{51}} I_2(6B)$$

where:

$\underline{I}_1 = \underline{y}$ intercept of $\underline{k}(1 - \epsilon)/\epsilon^3$ and

$\underline{I}_2 = \underline{y}$ intercept of $\underline{k}^{1/2}/\epsilon^3$.

For the time drive,

$$1A = 0.250.$$

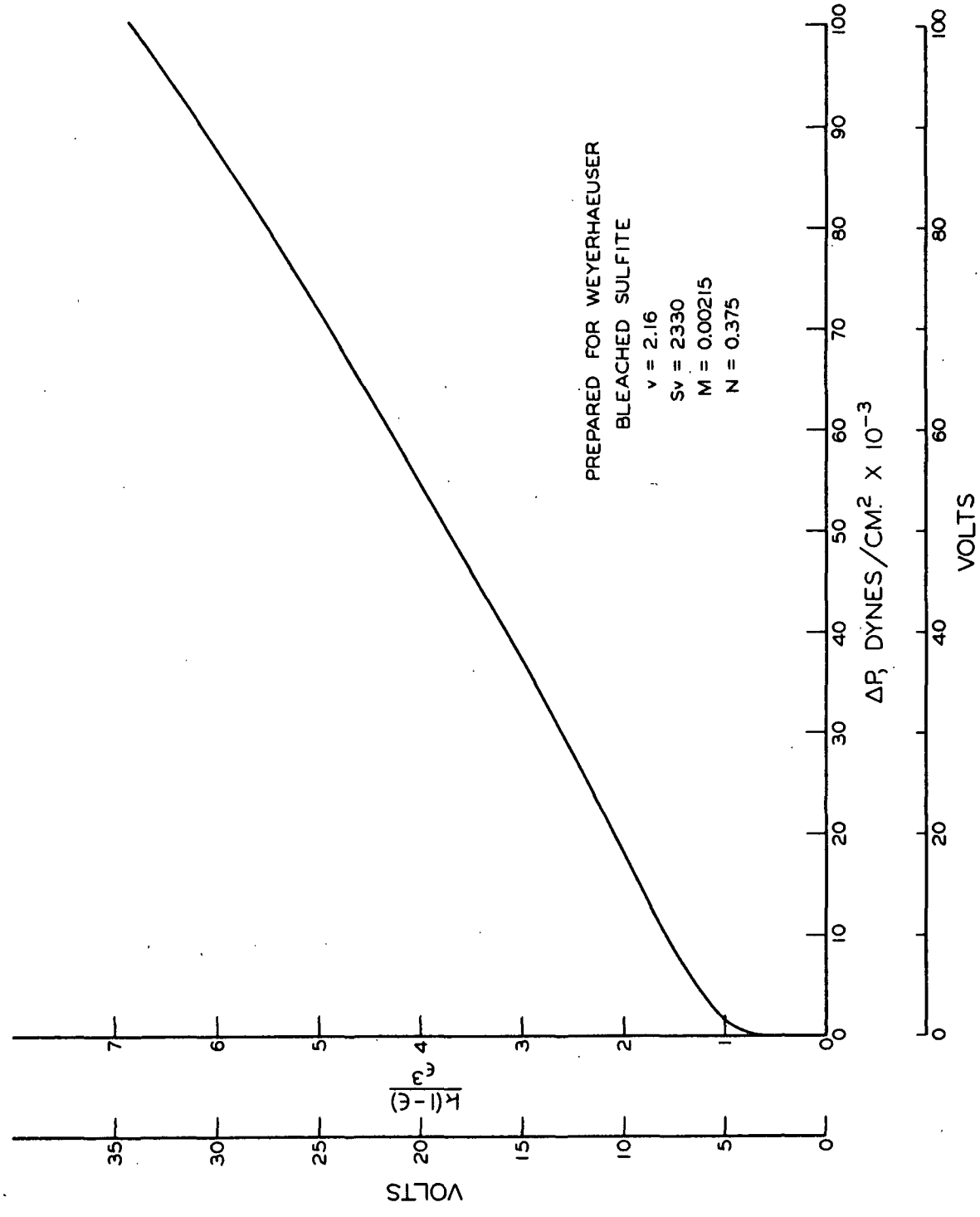

Figure 27. Porosity Function in Viscous Resistance

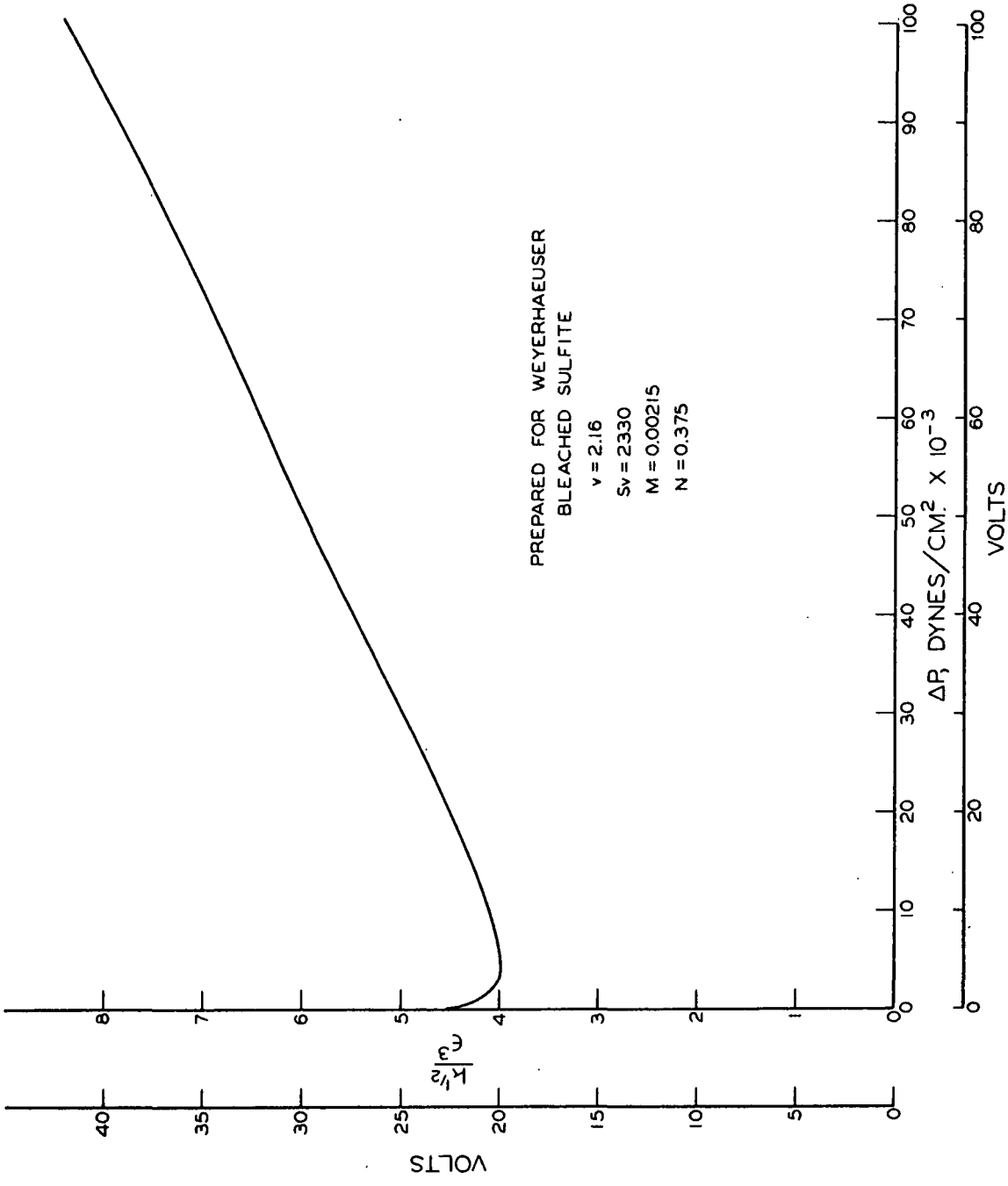

Figure 28. Porosity Function in Inertial Resistance

Thus, 8 sec. elapsed time = 100 volts

or 4 sec. problem time = 100 volts .

A slight modification is needed for velocities in the range $50 \leq \underline{U} \leq 100$ cm./sec. Here, the following scale factors were used:

$$100 \text{ volts} = 100{,}000 \text{ dynes/cm.}^2$$

$$\tau = 4t \text{ sec.}$$

Thus,

$$\frac{dV}{d\tau} = 0.25 \times 10^{-3} \frac{d\Delta P}{dt}$$

$$= 2.5 \times 10^{-3} v S_v \rho U^2 \left\{ \frac{\mu S_v}{50} \left[\frac{5k(1-\epsilon)}{\epsilon^3} \right] + \frac{0.1 U \rho}{50} \left(\frac{5k^{1/2}}{\epsilon^3} \right) \right\} \qquad \text{(VI-4)} .$$

As before, all capacitors were $1\mu f$, and values of resistors and potentiometer settings were:

$R_{51} = 1M$ $\qquad$ $6A = 2.5 \times 10^{-3} v S_v \rho U^2 \frac{R_{61}}{R_{62}}$

$R_{52} = 4M$ $\qquad$ $4B = \frac{\mu S_v}{50} R_{51} C_{51}$

$R_{53} = 20M$ $\qquad$ $6B = \frac{U}{500} R_{52} C_{51}$

$R_{54} = 10M$ $\qquad$ $7A = \frac{5 R_{53} C_{51} I_1}{100}$ (4B)

$R_{61} = 1M$ $\qquad$ $7B = \frac{5 R_{54} C_{51} I_2}{100} \frac{U}{500}$

$R_{62} = 6M$

For the time drive, $1A = 0.250$.

Thus, 8 sec. elapsed time = 100 volts

or 2 sec. problem time = 100 volts .

APPENDIX VII

DEVELOPMENT OF EMPIRICAL DATA CORRELATION

From Fig. 16 and 22, as a first approximation,

$$\Delta P = aU^n \quad \text{at constant basis weight, } W/A \tag{VII-1}$$

$$\Delta P = b(W/A)^m \quad \text{at constant velocity, } U \tag{VII-2}.$$

Therefore,

$$\Delta P = k'U^nW^m \tag{VII-3}$$

where a, b, k', m, and n are empirically determined constants.

Considering the case of constant-pressure filtrations of a dilute slurry with complete retention,

$$\frac{W}{A} = \rho s \frac{V}{A} \tag{VII-4}$$

$$U = \frac{1}{A}\frac{dV}{dt} \tag{VII-5}$$

where V is the total filtrate volume at time t.

Combining Equations (IV-3, -4, and -5) and integrating gives

$$t = \frac{(k')^{1/n}}{(1+m/n)\rho s}\Delta P^{-1/n}(W/A)^{1+m/n} \tag{VII-6}$$

where t is the time required to form a mat of basis weight W/A at a pressure drop maintained constant over the mat at ΔP.